Hindawi Publishing Corporation
EURASIP Journal on Advances in Signal Processing
Volume 2011, Article ID 857859, 17 pages
doi:10.1155/2011/857859

Research Article

Semiblind Channel Estimation for IFDMA in Case of Channels with Large Delay Spreads

Anja Sohl (EURASIP Member) and Anja Klein

Communications Engineering Lab, Technische Universität Darmstadt, Merckstraße 25, 64283 Darmstadt, Germany

Correspondence should be addressed to Anja Sohl, a.sohl@nt.tu-darmstadt.de

Received 15 April 2010; Revised 4 October 2010; Accepted 14 November 2010

Academic Editor: Hikmet Sari

Discrete Fourier Transform- (DFT-) precoded Orthogonal Frequency Division Multiple Access (OFDMA) with interleaved subcarrier allocation per user is considered which is denoted as Interleaved Frequency Division Multiple Access (IFDMA). For IFDMA, the received signal exhibits a cyclostationarity with the parameter Q which defines the number of allocated subcarriers per user. In previous works, we have shown that this cyclostationarity can be exploited for the application of subspace-based semiblind channel estimation to IFDMA. Nevertheless, the formerly proposed algorithm is restricted to channels with small delay spreads, meaning that the number of channel delay taps needs to be smaller than Q. In this paper, we introduce a new semiblind subspace-based channel estimation algorithm which identifies a subspace of the received signal that is spanned by the Q elements of the so-called cyclic channel impulse response. By doing so, the number of elements to be estimated is reduced and the proposed algorithm is able to cope with channels with large delay spreads.

1. Introduction

At present, research activities for beyond third generation (3G) of mobile radio systems are in progress worldwide. In this context, the International Telecommunication Union (ITU) has formulated a concept for the evolution of beyond 3G mobile radio systems which is denoted as International Mobile Telecommunications- (IMT-) Advanced [1]. For the uplink of future mobile radio systems, several multiple access schemes are under discussion as candidates including Orthogonal Frequency Division Multiple Access (OFDMA) because of its favorable properties that have been described, for example, in [2]. Other promising multiple access schemes result from the application of a Discrete Fourier Transform (DFT) precoding to OFDMA. In this work, the focus is on DFT-precoded OFDMA with interleaved subcarrier allocation resulting in the well-known Interleaved Frequency Division Multiple Access (IFDMA) scheme [3, 4]. Compared to OFDMA, the IFDMA scheme provides higher-frequency diversity as the data symbols are spread over subcarriers that are distributed over the total available bandwidth [4]. Further on, the IFDMA transmit signal exhibits a very low Peak-to-Average Power Ratio (PAPR) which is beneficial in terms of the application of cost-efficient high-power amplifiers in the mobile terminals [5]. Due to its favorable properties IFDMA is well suitable for the nonadaptive uplink transmission and has attracted great interest during the last years within the European WINNER project representing one major effort for the development of an IMT-Advanced compliant radio interface [6].

The IFDMA signal generation can be described in time domain as a compression, repetition, and subsequent user dependent phase rotation of blocks of Q-modulated data symbols and, thus, is very efficient in terms of implementation issues and leads to a low PAPR of the IFDMA transmit signal enabling the application of low-cost amplifiers [3, 7]. Moreover, the IFDMA signal generation leads to a transmit signal which exhibits redundancy and a cyclostationarity

with Q. In frequency domain, the data of a certain user is transmitted on a specific set of subcarriers that are equidistantly distributed over the bandwidth. Due to transmission on distributed subcarriers, IFDMA provides high-frequency diversity [8]. However, during uplink transmission, the pilot-assisted estimation of channel variations in frequency domain with the help of interpolation between adjacent subcarriers allocated to a certain user raises difficulties as the sampling theorem in frequency domain cannot be fulfilled especially for low data rates, that is, a large distance between the allocated subcarriers [9]. Thus, for IFDMA, the reduction of pilot symbol overhead with the help of interpolation in frequency domain is not feasible, in general. The missing possibility of interpolation in frequency domain even for channels with low-frequency selectivity, that is, a small delay spread in time domain, leads to a high pilot symbol overhead concerning the estimation of channel variations in frequency domain for IFDMA uplink transmission [10].

In order to reduce the pilot symbol overhead in frequency domain, the estimation of frequency domain channel variations with the help of subspace-based semiblind channel estimation is an appropriate approach. Subspace-based algorithms are principally based on redundancy existent in the received signal. In [11–13], subspace-based channel estimation has been introduced for single-carrier systems, in general, where the redundancy in the received signal is introduced according to different strategies. In [13], the redundancy is introduced at the receiver by either an oversampling of the signal at a single receiver or considering the same signal at multiple receivers. In [11, 12], redundancy is introduced at the transmitter via a specific precoding. The principle of subspace-based estimation has been combined with pilot-assisted channel estimation leading to the subspace-based semiblind channel estimation and has been further extended to the application in an Orthogonal Frequency Division Multiplexing (OFDM) system where either the redundancy inherent in the cyclic prefixes is exploited [14, 15] or the redundancy is introduced via precoding at the transmitter, [16].

In our previous work [17, 18], we presented a subspace-based channel estimation algorithm for IFDMA which takes advantage of the special signal structure in time domain. Due to the characterization of IFDMA signal generation by compression, repetition, and phase shifting, it is apparent that the signal inherently contains redundancy and that a subspace analysis of the received IFDMA signal is feasible without any modification at the transmitter or oversampling at the receiver. However, the subspace-based algorithm introduced in [17, 18] is constrained in terms of the number of unknowns that can be estimated. Each received IFDMA symbol exhibits a cyclostationarity with the parameter Q and, thus, a maximum number of Q unknowns, more specifically a maximum number of Q channel delay taps, can be estimated. If the number L_C of channel delay taps is larger than the number Q of allocated subcarriers per user, that is, $L_C > Q$, the previously introduced semiblind subspace-based channel estimation is not feasible.

In this paper, we introduce a semiblind subspace-based channel estimation algorithm which is capable to estimate channels with an arbitrary number of channel delay taps and, thus, overcomes the restriction of channels with small delay spreads adhering to the algorithms in [17, 18]. This new algorithm considers the channel influence on the received IFDMA signal from a different perspective compared to the formerly presented algorithms. The channel influence on each received IFDMA symbol can be fully described by Q channel transfer factors corresponding to the Q allocated subcarriers in frequency domain. In time domain, this is equivalent of the description of Q-transmitted data symbols which are distorted by a so-called cyclic channel impulse response. This cyclic channel impulse response contains the user specific phase shift and represents the time domain equivalent to the Q channel transfer factors in frequency domain. The objective of our proposed algorithm is the estimation of the Q elements of the cyclic channel impulse response despite the well-known estimation of the L_C ordinary channel delay taps. For this purpose, the received IFDMA signal is analyzed for a subspace that is spanned by the introduced cyclic channel impulse response. The parts of the received signal comprising this subspace are identified and are subjected to a subspace analysis. Then an algorithm is derived which computes the desired Q elements of the cyclic channel impulse response representing the time domain equivalent of the Q channel transfer factors in frequency domain. By this means, the channel is identifiable for an arbitrary number of delay taps and the new algorithm opens up the possibility to apply semiblind subspace-based channel estimation to IFDMA without any restriction concerning the delay spread of the channel.

The semiblind subspace-based channel estimation can be combined with decision-directed channel estimation in order to estimate the channel variations in time domain as it has been presented in [18] for the case of channels with small delay spreads. In this paper, the previously described principle is applied to the new semiblind subspace-based channel estimation for channels with large delay spread in order to estimate the channel variations in frequency and time domain. By this means, the channel can be estimated even if the sampling theorem in frequency and time domain is not fulfilled and current channel estimation approaches fail.

In the following, the new subspace-based semiblind channel estimation for the estimation of channel variations in frequency domain is derived mathematically and numerical results are presented evaluating the performance of this algorithm. The performance of decision-directed channel estimation with the new subspace-based semiblind channel estimation as initialization is also compared to pilot-assisted channel estimation. Finally, the proposed algorithm is investigated in terms of computational complexity.

The rest of the paper is organized as follows. In Section 2, the IFDMA system model is described and the IFDMA signal generation is presented in frequency as well as in time domain. In Section 3, pilot and data multiplexing is explained. In Section 4, the subspace-based semiblind channel estimation for the case of channels with large delay spreads is derived and its combination with decision-directed channel estimation is explained. In Section 5, the

performance of the introduced semiblind channel estimation is evaluated based on a mean square error and a complexity analysis. Section 6 concludes the work.

2. IFDMA System Model

2.1. Transmitter. In this section, the signal generation of IFDMA is presented. In the following, all signals are represented by their discrete-time equivalents in the complex baseband. Vectors and matrices are denoted by lower and upper case boldfaced letters, respectively. $\mathbf{F}_{\mathrm{A}}$ represents an $A\times A$ DFT matrix with the elements $[\mathbf{F}_{\mathrm{A}}]_{i,m}$, $i,m = 0,\ldots,Q-1$, calculated by

$$[\mathbf{F}_{\mathrm{A}}]_{i,m} = \frac{1}{\sqrt{A}} \cdot e^{-j2\pi im/A}. \tag{1}$$

Further notations used throughout this work are given in Table 1.

For IFDMA signal generation, Q data symbols that are transmitted by a certain user are combined in a block of data symbols. The input of the IFDMA signal generator is given by the kth block, $k = 0,\ldots,K-1$, which consists of Q data symbols $d_{k,q}^{(u)}$, $q = 0,\ldots,Q-1$, that are transmitted at data symbol rate $1/T_{\mathrm{S}}$ by the user with index u, $u = 0,\ldots,U-1$ and is denoted by

$$\mathbf{d}_k^{(u)} = \left[d_{k,0}^{(u)},\ldots,d_{k,Q-1}^{(u)}\right]^{\mathrm{T}}. \tag{2}$$

The data symbols $d_{k,q}^{(u)}$ result from coded and interleaved data bits that are mapped according to a bit mapping scheme like Phase Shift Keying (PSK) or Quadrature Amplitude Modulation (QAM). Further on, the data symbols $d_{k,q}^{(u)}$ are assumed to be independently identically distributed (i.i.d.) with $\mathrm{E}\{|d_{k,q}^{(u)}|^2\} = \sigma_{\mathrm{D}}^2$ and zero-mean. The output of the IFDMA signal generator which results from the kth block $\mathbf{d}_k^{(u)}$ is denoted by the kth IFDMA symbol $\mathbf{x}_k^{(u)}$. The mathematical relations between $\mathbf{d}_k^{(u)}$ and $\mathbf{x}_k^{(u)}$ are derived in Sections 2.1.1 and 2.1.2. The IFDMA signal generation can be described in frequency as well as in time domain. As both descriptions are equivalent and of relevance for the remainder of this work, the IFDMA signal generation is explained in frequency and time domain in the following.

2.1.1. IFDMA Signal Generation in Frequency Domain. This section presents the IFDMA signal generation in frequency domain according to [4]. In Figure 1, the block diagram of the IFDMA signal generation in frequency domain and subsequent Cyclic Prefix (CP) insertion are illustrated. First, the block $\mathbf{d}_k^{(u)}$ of data symbols is DFT precoded. Then, the precoded elements are assigned to a user specific set of Q subcarriers which are equidistantly distributed over the total number $N = L_{\mathrm{U}} \cdot Q$, $L_{\mathrm{U}} \in \mathbb{Z}$, of available subcarriers in the system. The subcarrier assignment can be described by an $N \times Q$ mapping matrix $\mathbf{M}^{(u)}$ which is characterized by its

Table 1: Notations.

$(\cdot)^*$	Conjugate complex of a vector/matrix
$(\cdot)^{\mathrm{T}}$	Transpose of a vector/matrix
$(\cdot)^{\mathrm{H}}$	Hermitian of a vector/matrix
$\mathrm{E}\{\cdot\}$	Expectation of a vector/matrix
$\mathrm{diag}\{\mathbf{a}\}$	Diagonal matrix having the vector $\mathbf{a}$ as its main diagonal
$\mathbf{I}_\nu$	$\nu \times \nu$ identity matrix
$\mathbf{0}_a$	$a \times a$ matrix containing all zero elements
$\mathbf{0}_{a\times b}$	$a \times b$ matrix containing all zero elements
$\lfloor a \rfloor$	nearest integer smaller than or equal to a
$\square$	matrix or vector entries which are of no relevance for subsequent derivations.

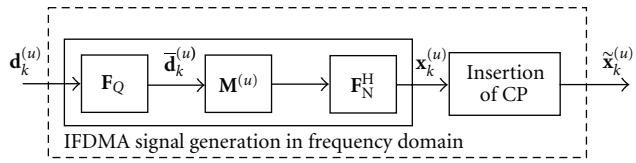

Figure 1: Block diagram of IFDMA signal generation in frequency domain and CP insertion.

elements $[\mathbf{M}^{(u)}]_{n,q}$, with $n = 0,\ldots,N-1$ and $q = 0,\ldots,Q-1$, that are given by

$$\left[\mathbf{M}^{(u)}\right]_{n,q} = \begin{cases} 1, & \text{for } n = q \cdot L_{\mathrm{U}} + u, \\ 0, & \text{else} \end{cases} \tag{3}$$

(see [4]). Afterwards, an Inverse Discrete Fourier Transform (IDFT) operation is applied to the precoded and mapped data symbols in order to get a time domain signal vector at the output of the IFDMA signal generator. The DFT-precoded, mapped, and IDFT-transformed block of data symbols is represented as

$$\mathbf{x}_k^{(u)} = \mathbf{F}_{\mathrm{N}}^{\mathrm{H}} \cdot \mathbf{M}^{(u)} \cdot \mathbf{F}_{\mathrm{Q}} \cdot \mathbf{d}_k^{(u)} = \left[x_{k,0}^{(u)},\ldots,x_{k,N-1}^{(u)}\right]^{\mathrm{T}} \tag{4}$$

(see [4]). $\mathbf{x}_k^{(u)}$ denotes the kth IFDMA symbol of a user with index u with the elements $x_{k,n}^{(u)}$, $n = 0,\ldots,N-1$, transmitted at chip rate $1/T_{\mathrm{C}} = L_{\mathrm{U}}/T_{\mathrm{S}}$.

In order to avoid intersymbol and intercarrier interference, a CP consisting of $N_{\mathrm{G}} = L_{\mathrm{G}} \cdot Q$ elements and with a duration that is larger than the maximum delay of the channel is inserted in-between successive IFDMA symbols [2]. L_{G} is chosen such that $N_{\mathrm{G}} \in \mathbb{Z}$. The IFDMA symbol including CP is denoted by $\tilde{\mathbf{x}}_k^{(u)}$. In time domain, the data symbols of different users are additionally separated by the transmission within different Time Division Multiple Access (TDMA) slots. Each TDMA slot consists of K successively transmitted IFDMA symbols plus CP and exhibits a time duration $K \cdot T$. That is, the data of a user under consideration is transmitted on a user-specific set of Q subcarriers in frequency domain and within K successively transmitted IFDMA symbols in time domain. For each user terminal, this opens up the possibility to enter a microsleep mode during

the transmission phase of the other users. This microsleep mode is beneficial in terms of the power consumption of the mobile terminal because, by this means, considerable energy savings can be achieved for each users' mobile terminal [19–21].

2.1.2. IFDMA Signal Generation in Time Domain. This section presents the equivalent IFDMA signal generation in time domain whose principle has been introduced in [3]. In Figure 2, the block diagram of the IFDMA signal generation in time domain is illustrated.

First, the block $\mathbf{d}_k^{(u)}$ of data symbols with a duration of $Q \cdot T_S$ is compressed in time domain by the factor $L_U = N/Q$ [3]. The resulting compressed block is denoted by

$$\mathbf{w}_k^{(u)} = \left[w_{k,0}^{(u)}, \ldots, w_{k,Q-1}^{(u)}\right]. \tag{5}$$

The elements $w_{k,q}$, $q = 0, \ldots, Q-1$, are transmitted at chip rate $1/T_C = L_U/T_S$ and have the average power $E\{|w_{k,q}^{(u)}|^2\} = \sigma_W^2$. Subsequently, $\mathbf{w}_k^{(u)}$ is repeated L_U-times. After compression and repetition, a user-dependent phase shift is applied in order to assure the orthogonality between the signals of different users. With $\varphi^{(u)} = u \cdot 2\pi/N$ the user-dependent phase [3], the phase shift matrices $\mathbf{\Phi}_i^{(u)}$, $i = 0, \ldots, L_U - 1$, are defined as diagonal matrices according to

$$\mathbf{\Phi}_i^{(u)} = \begin{bmatrix} e^{-j\cdot(i\cdot Q)\cdot\varphi^{(u)}} & 0 & \cdots & 0 \\ 0 & \ddots & & \vdots \\ \vdots & & & 0 \\ 0 & \cdots & 0 & e^{-j\cdot(i\cdot Q+Q-1)\cdot\varphi^{(u)}} \end{bmatrix}. \tag{6}$$

Then, the kth IFDMA symbol $\mathbf{x}_k^{(u)}$ of the user with index u is calculated by

$$\mathbf{x}_k^{(u)} = \begin{bmatrix} x_{k,0}^{(u)} \\ \vdots \\ x_{k,N-1}^{(u)} \end{bmatrix} = \begin{bmatrix} \mathbf{\Phi}_0^{(u)} \\ \vdots \\ \mathbf{\Phi}_{L_U-1}^{(u)} \end{bmatrix} \cdot \mathbf{w}_k^{(u)}. \tag{7}$$

According to [3, 4], the IFDMA symbol $\mathbf{x}_k^{(u)}$ in (7) is equivalent to the IFDMA symbol in (4).

Finally, $\mathbf{x}_k^{(u)}$ is extended by a CP as explained in Section 2.1.1. In analogy to (7), the extension of $\mathbf{x}_k^{(u)}$ by a CP can be represented by

$$\tilde{\mathbf{x}}_k^{(u)} = \begin{bmatrix} \mathbf{\Phi}_{L_U-L_G-1}^{(u)} \\ \vdots \\ \mathbf{\Phi}_{L_U-1}^{(u)} \\ \mathbf{\Phi}_0^{(u)} \\ \vdots \\ \mathbf{\Phi}_{L_U-1}^{(u)} \end{bmatrix} \cdot \mathbf{w}_k^{(u)}. \tag{8}$$

Again, K IFDMA symbols with CP are transmitted within a TDMA slot.

2.2. Mobile Radio Channel. In this section, a model for the mobile radio channel is presented. The physical effects that occur during free-space propagation in a mobile scenario are modeled based on a discrete, linear time-variant system in the equivalent baseband. During uplink transmission, different users experience different channel conditions and, thus, the different delay paths are represented by L_C time-variant and user-dependent channel coefficients in the following. It is assumed that the channel delay coefficients stay constant within the duration T of one IFDMA symbol including CP and are changing for each IFDMA symbol with index $k = 0, \ldots, K-1$. It is assumed that the delay time τ_l of the lth delay path, with $l = 0, \ldots, L-1$, can be expressed as an integer multiple of the chip duration T_C, that is, $\tau_l = \nu \cdot T_C$ with $\nu \in \mathbb{N}$ and $l = 0, \ldots, L_C - 1$. Then, the maximum delay time τ_{max} of the channel is given by

$$\tau_{max} = L_C \cdot T_C. \tag{9}$$

The frequency variations of the mobile radio channel are characterized with the help of the coherence bandwidth B_{coh} that determines the bandwidth for which the channel characteristics are correlated and is approximated by

$$B_{coh} \approx \frac{1}{\tau_{max}} \tag{10}$$

(see [22]). The time variations of the mobile radio channel are characterized with the help of the coherence time T_{coh} that determines the time duration for which the channel characteristics can be considered as time-invariant. With v being the velocity of the mobile terminal, c the speed of light, and f_0 the carrier frequency of the system, the maximum Doppler shift is calculated by $f_{D,max} = v \cdot f_0/c$ and determines the coherence time approximately by

$$T_{coh} \approx \frac{1}{2 \cdot f_{D,max}} \tag{11}$$

(see [22]). The IFDMA symbols $\tilde{\mathbf{x}}_k^{(u)}$, $k = 0, \ldots, K-1$, each containing a CP with a time duration $N_G \cdot T_C$ that is larger than the maximum delay τ_{max} of the mobile radio channel, are transmitted over the channel with L delay paths. With $N_G > L_C$ and $N > N_G > L_C$, an $N \times 1$ channel impulse response vector $\mathbf{h}_k^{(u)}$ containing the channel delay coefficients $h_{k,l}^{(u)}$ is defined according to

$$\mathbf{h}_k^{(u)} = \left[h_{k,0}^{(u)}, \ldots, h_{k,L_C-1}^{(u)}, \underbrace{0, \ldots, 0}_{N-L_C}\right]^T. \tag{12}$$

The application of an N-point DFT to the vector $\mathbf{h}_k^{(u)}$ according to

$$\overline{\mathbf{h}}_k^{(u)} = \mathbf{F}_N \cdot \mathbf{h}_k^{(u)} \tag{13}$$

leads to a vector $\overline{\mathbf{h}}_k^{(u)} = [\overline{h}_{k,0}^{(u)}, \ldots, \overline{h}_{k,N-1}^{(u)}]^T$ containing N coefficients of the time-variant channel transfer function.

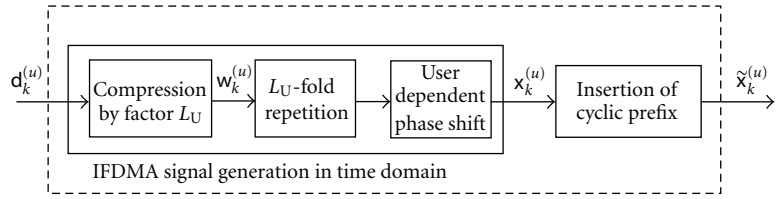

Figure 2: Block diagram of IFDMA signal generation in time domain and cyclic prefix insertion.

2.3. Receiver. In this section, the influence of the mobile radio channel on the demodulated IFDMA signal is explained. The IFDMA signal demodulation is given in frequency domain which represents the description corresponding to the IFDMA signal generation in Section 2.1.1. In Figure 3, the IFDMA signal demodulation is embedded in the discrete-time transmission chain illustrating the IFDMA signal generation at the transmitter, (compare Section 2.1.1), the transmission over the mobile radio channel, distortion by AWGN, and the IFDMA signal demodulation at the receiver.

In the following, exact frequency and time synchronization between mobile station and base station is assumed. The IFDMA symbol $\tilde{\mathbf{x}}_k^{(u)}$ plus CP that is received after transmission over the mobile radio channel with impulse response vector $\mathbf{h}_k^{(u)}$ and distortion by the AWGN vector $\tilde{\boldsymbol{\nu}}_k^{(u)} = [\nu_{k,0}^{(u)}, \ldots, \nu_{k,N+N_G-1}^{(u)}]$ whose elements have the average power σ_ν^2 is denoted by $\tilde{\mathbf{r}}_k^{(u)}$. Due to CP insertion, the interference between successively transmitted IFDMA symbols is avoided and the transmission over the channel can be explained for a single IFDMA symbol independently from the other IFDMA symbols. At the receiver, the CP part of $\tilde{\mathbf{r}}_k^{(u)}$ is discarded and $\mathbf{r}_k^{(u)}$ denotes the $N \times 1$ received IFDMA symbol vector.

$\mathbf{r}_k^{(u)}$ can be described as a function of the transmitted IFDMA symbol $\mathbf{x}_k^{(u)}$, the mobile radio channel with impulse response vector $\mathbf{h}_k^{(u)}$, and the AWGN vector $\boldsymbol{\nu}_k^{(u)} = [\nu_{k,N_G}^{(u)}, \ldots, \nu_{k,N+N_G-1}^{(u)}]^T$. With $\mathbf{H}_k^{(u)}$ being the $N \times N$ right circulant matrix having $\mathbf{h}_k^{(u)}$ as its first column, the received IFDMA symbol $\mathbf{r}_k^{(u)}$ is given by

$$\mathbf{r}_k^{(u)} = \mathbf{H}_k^{(u)} \cdot \mathbf{x}_k^{(u)} + \boldsymbol{\nu}_k^{(u)} \tag{14}$$

(see [23, 24]). The demodulation of $\mathbf{r}_k^{(u)}$ is performed by the application of an N-point DFT matrix $\mathbf{F}_N$, the demapping matrix $\mathbf{M}^{(u)^T}$, and a Q-point IDFT matrix $\mathbf{F}_Q^H$ to $\mathbf{r}_k^{(u)}$ according to

$$\mathbf{y}_k^{(u)} = \mathbf{F}_Q^H \cdot \mathbf{M}^{(u)^T} \cdot \mathbf{F}_N \cdot \mathbf{r}_k^{(u)} \tag{15}$$

(see [24]). For $k = 0, \ldots, K-1$ and $q = 0, \ldots, Q-1$, let the elements $c_{k,q}^{(u)}$ be calculated based on the elements $h_{k,n}^{(u)}$, $n = 0, \ldots, N-1$, of the channel impulse response vector according to

$$c_{k,q}^{(u)} = \sum_{i=0}^{L_U-1} h_{k,iQ+q}^{(u)} \cdot e^{j \cdot (2 \cdot \pi/N) \cdot u \cdot (i \cdot Q + q)} \tag{16}$$

(see [25]). Then, the matrix

$$\mathcal{H}_k^{(u)} = \mathbf{F}_Q^H \cdot \mathbf{M}^{(u)^T} \cdot \mathbf{F}_N \cdot \mathbf{H}_k^{(u)} \cdot \mathbf{F}_N^H \cdot \mathbf{M}^{(u)} \cdot \mathbf{F}_Q \tag{17}$$

refers to a $Q \times Q$ right circulant matrix having the vector $\mathbf{c}_k^{(u)} = [c_{k,0}^{(u)}, \ldots, c_{k,Q-1}^{(u)}]^T$ as its first column [24]. The elements $c_{k,q}^{(u)}$ are referred to as the elements of the cyclic channel impulse response in the remainder of this work. With

$$\mathbf{v}_k^{(u)} = \mathbf{F}_Q^H \cdot \mathbf{M}^{(u)^T} \cdot \mathbf{F}_N \cdot \boldsymbol{\nu}_k^{(u)} \tag{18}$$

denoting the noise vector after IFDMA signal demodulation, the demodulated IFDMA symbol $\mathbf{y}_k^{(u)}$ is described in dependency of the matrix $\mathcal{H}_k^{(u)}$ containing the elements of the cyclic channel impulse response by

$$\mathbf{y}_k^{(u)} = \mathcal{H}_k^{(u)} \cdot \mathbf{d}_k^{(u)} + \mathbf{v}_k^{(u)}. \tag{19}$$

Thus, the transmission chain illustrated in Figure 3 can be represented based on the cyclic channel impulse response by the equivalent transmission chain depicted in Figure 4.

The demodulated IFDMA symbol $\overline{\mathbf{y}}_k^{(u)}$ in frequency domain is given by

$$\overline{\mathbf{y}}_k^{(u)} = \mathbf{F}_Q \cdot \mathcal{H}_k^{(u)} \cdot \mathbf{d}_k^{(u)} + \mathbf{F}_Q \cdot \mathbf{v}_k^{(u)}. \tag{20}$$

In [26], it has been shown that premultiplication with a $Q \times Q$ DFT matrix and postmultiplication with a $Q \times Q$ IDFT matrix of a $Q \times Q$ circulant matrix $\mathcal{H}_k^{(u)}$ leads to a diagonalized matrix. Thus, according to [26],

$$\overline{\mathcal{H}}_k^{(u)} = \mathbf{F}_Q \cdot \mathcal{H}_k^{(u)} \cdot \mathbf{F}_Q^H \tag{21}$$

is a $Q \times Q$ diagonal matrix having the vector

$$\overline{\mathbf{c}}_k^{(u)} = \mathbf{F}_Q \cdot \mathbf{c}_k^{(u)} = \left[\overline{c}_{k,0}^{(u)}, \ldots, \overline{c}_{k,Q-1}^{(u)}\right]^T \tag{22}$$

as its main diagonal.

Under consideration of (21), (20) can be rewritten according to

$$\overline{\mathbf{y}}_k^{(u)} = \overline{\mathcal{H}}_k^{(u)} \cdot \overline{\mathbf{d}}_k^{(u)} + \overline{\mathbf{v}}_k^{(u)}, \tag{23}$$

showing that each subcarrier is affected by a flat fading channel that can be described by the complex factor $\overline{c}_{k,q}^{(u)}$ which is denoted by the qth channel transfer factor corresponding to the subcarrier with index $q \cdot L_U + u$ and the IFDMA symbol with index k in the following.

According to (23), an estimate for the transmitted data symbols $\mathbf{d}_k^{(u)}$ can be obtained if the matrix $\overline{\mathcal{H}}_k^{(u)}$ and, thus, the Q channel transfer factors $\overline{c}_{k,q}^{(u)}$ are known at the receiver. In a practical system, the channel transfer factors $\overline{c}_{k,q}^{(u)}$ are unknown and, therefore, estimates have to be utilized for data estimation. The estimation of the Q channel transfer factors is addressed in the remainder of this work.

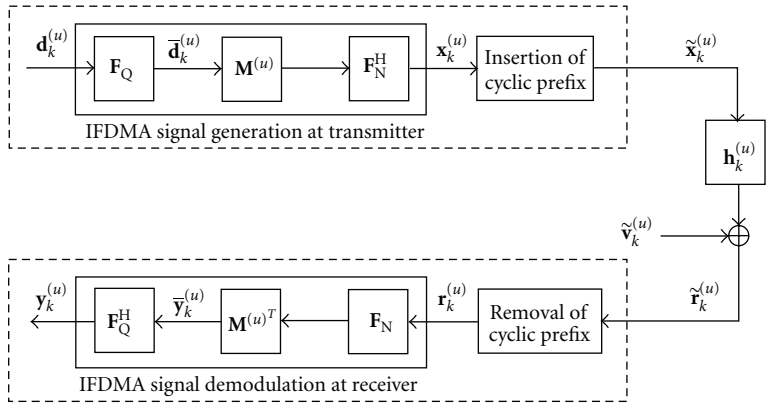

Figure 3: Discrete-time transmission chain.

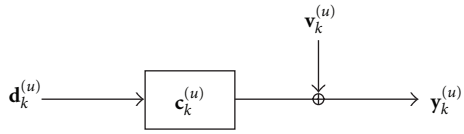

Figure 4: Equivalent transmission chain.

3. Subcarrier-Wise Pilot Insertion

For subcarrier-wise pilot insertion, a subset of Q_P subcarriers out of the total number Q of subcarriers allocated to a certain user in the IFDMA symbol with index $k = \kappa$ is utilized for pilot transmission. The remaining $Q_\mathrm{D} = Q - Q_\mathrm{P}$ subcarriers are exploited by transmitting data symbols within the κth IFDMA symbol. In the following, the insertion of pilot symbols is explained based on the IFDMA signal generation in frequency domain presented in Section 2.1.1, due to the simplicity of this model.

The sequence $\boldsymbol{\rho}^{(u)} = [\rho_0^{(u)}, \ldots, \rho_{Q_\mathrm{P}-1}^{(u)}]^\mathrm{T}$ contains Q_P pilot symbols which are taken from a Constant Amplitude Zero Autocorrelation (CAZAC) sequence and have an average power $\mathrm{E}\{|\rho_q^{(u)}|^2\} = \sigma_\mathrm{P}^2$. $\boldsymbol{\rho}^{(u)}$ is multiplied by a $Q_\mathrm{P} \times Q_\mathrm{P}$ DFT matrix $\mathbf{F}_{Q_\mathrm{P}}$. The resulting sequence $\overline{\boldsymbol{\rho}}^{(u)}$ of pilot symbols in frequency domain is given by

$$\overline{\boldsymbol{\rho}}^{(u)} = \mathbf{F}_{Q_\mathrm{P}} \cdot \boldsymbol{\rho}^{(u)} = \left[\overline{\rho}_0^{(u)}, \ldots, \overline{\rho}_{Q_\mathrm{P}-1}^{(u)}\right]^\mathrm{T}. \tag{24}$$

The elements $\overline{\rho}_{q_\mathrm{P}}^{(u)}$, $q_\mathrm{P} = 0, \ldots, Q_\mathrm{P} - 1$, are mapped onto a subset consisting of Q_P equidistantly spaced subcarriers out of the total number Q of subcarriers allocated to the user. The number Q_P of subcarriers that are used for pilot transmission is calculated by

$$Q_\mathrm{P} = \frac{Q}{I}, \tag{25}$$

where I denotes the interpolation depth in frequency domain and is chosen such that $Q_\mathrm{P} \in \mathbb{Z}$. That means, for example, for $I = 2$, every second subcarrier that is allocated to a specific user is utilized for pilot transmission.

The elements $\overline{\rho}_{q_\mathrm{P}}^{(u)}$, with $q_\mathrm{P} = 0, \ldots, Q_\mathrm{P} - 1$, are transmitted on subcarriers with indices

$$\eta(q_\mathrm{P}) = q_\mathrm{P} \cdot L_\mathrm{U} \cdot I + u. \tag{26}$$

which are denoted by the pilot carrying subcarriers in the following. The allocation of the elements $\overline{\rho}_{q_\mathrm{P}}^{(u)}$ to the Q_P pilot carrying subcarriers is performed by the application of the pilot mapping matrix $\mathbf{M}_\mathrm{P}^{(u)}$ whose elements $[\mathrm{M}_\mathrm{P}^{(u)}]_{n,q_\mathrm{P}}$ for $n = 0, \ldots, N - 1$ and $q_\mathrm{P} = 0, \ldots, Q_\mathrm{P} - 1$ are given by

$$\left[\mathbf{M}_\mathrm{P}^{(u)}\right]_{n,q_\mathrm{P}} = \begin{cases} 1, & \text{for } n = \eta(q_\mathrm{P}), \\ 0, & \text{else.} \end{cases} \tag{27}$$

Simultaneously, the sequence $\boldsymbol{\delta}_\kappa^{(u)} = [d_{\kappa,0}^{(u)}, \ldots, d_{\kappa,Q_\mathrm{D}-1}^{(u)}]^\mathrm{T}$ of data symbols with average power $\mathrm{E}\{|d_{\kappa,q}^{(u)}|^2\} = \sigma_\mathrm{D}^2$ is multiplied by a $Q_\mathrm{D} \times Q_\mathrm{D}$ DFT matrix $\mathbf{F}_{Q_\mathrm{D}}$. The resulting sequence $\overline{\boldsymbol{\delta}}_\kappa^{(u)}$ of data symbols in frequency domain is given by

$$\overline{\boldsymbol{\delta}}_\kappa^{(u)} = \mathbf{F}_{Q_\mathrm{D}} \cdot \boldsymbol{\delta}_\kappa^{(u)} = \left[\overline{d}_{\kappa,0}^{(u)}, \ldots, \overline{d}_{\kappa,Q_\mathrm{D}-1}^{(u)}\right]^\mathrm{T}. \tag{28}$$

The elements $\overline{d}_{\kappa,0}^{(u)}$, $q_\mathrm{D} = 0, \ldots, Q_\mathrm{D} - 1$, are transmitted on the Q_D subcarriers with indices

$$\zeta(q_\mathrm{D}) = \left\lfloor \frac{q_\mathrm{D}}{I-1} \right\rfloor \cdot L_\mathrm{U} \cdot (I-1) + L_\mathrm{U} \cdot (q_\mathrm{D}+1) + u, \tag{29}$$

which are denoted by the nonpilot carrying subcarriers in the following. The allocation of the elements $\overline{d}_{\kappa,0}^{(u)}$, $q_\mathrm{D} = 0, \ldots, Q_\mathrm{D} - 1$, to the remaining Q_D nonpilot carrying subcarriers is realized by the data mapping matrix $\mathbf{M}_\mathrm{D}^{(u)}$ with the elements $[\mathbf{M}_\mathrm{D}^{(u)}]_{n,q_\mathrm{D}}$ for $n = 0, \ldots, N - 1$ given by

$$\left[\mathbf{M}_\mathrm{D}^{(u)}\right]_{n,q_\mathrm{D}} = \begin{cases} 1, & \text{for } n = \zeta(q_\mathrm{D}), \\ 0, & \text{else.} \end{cases} \tag{30}$$

The superposition of the mapped pilot and mapped data symbols is multiplied by an $N \times N$ IDFT matrix $\mathbf{F}_\mathrm{N}^\mathrm{H}$. Then, the IFDMA symbol $\mathbf{x}_\kappa^{(u)}$ containing pilot and data symbols is given by

$$\mathbf{x}_\kappa^{(u)} = \mathbf{F}_\mathrm{N}^\mathrm{H} \cdot \left(\mathbf{M}_\mathrm{P}^{(u)} \cdot \mathbf{F}_{Q_\mathrm{P}} \cdot \boldsymbol{\rho}^{(u)} + \mathbf{M}_\mathrm{D}^{(u)} \cdot \mathbf{F}_{Q_\mathrm{D}} \cdot \boldsymbol{\delta}_\kappa^{(u)}\right). \tag{31}$$

Finally, $\mathbf{x}_\kappa^{(u)}$ is expanded by a CP with N_G elements and the resulting IFDMA symbol with CP $\tilde{\mathbf{x}}_\kappa^{(u)}$ is transmitted over the mobile radio channel.

In order to estimate the channel variations in frequency domain with pure pilot-assisted channel estimation, at least one pilot carrying subcarrier per coherence bandwidth B_{coh} is required which entails the usage of $Q_P = Q$ pilot carrying subcarriers if $Q < 2 \cdot L_C$. The channel variations in time domain with pure pilot-assisted channel estimation entail the usage of at least 2 pilot carrying IFDMA symbols per TDMA slot in order to apply interpolation filtering.

In the following, it is assumed that the distance between neighboring pilot carrying subcarriers is larger than B_{coh} and that there is only one pilot carrying IFDMA symbol per TDMA slot.

4. Semiblind Channel Estimation

4.1. Estimation of Frequency Domain Channel Variations. In this section, subspace-based semiblind channel estimation is derived for the case of $L_C > Q$ of channel delay taps. In general, the cp consists of $N_G = L_G \cdot Q$ elements with

$$L_G = \left\lceil \frac{L_C}{Q} \right\rceil. \tag{32}$$

The algorithm explained in [18] provides estimates for the L_C delay taps of the channel impulse response vector $\mathbf{h}_k^{(u)}$. As each received IFDMA is cyclostationary with Q, a maximum number of $L_C \leq Q$ channel delay taps can be estimated. That is, for $L_C > Q$, the estimation of the channel delay taps $h_{k,0}^{(u)}, \ldots, h_{k,L_C-1}^{(u)}$ is not feasible while applying the subspace-based semiblind channel estimation introduced in [18]. However, for IFDMA the knowledge of the Q channel transfer coefficients corresponding to the allocated subcarriers is sufficient to describe the channel influence on the received IFDMA symbol. Therefore, in the following, the subspace-based semiblind channel estimation is derived in order to estimate the elements $c_{k,q}^{(u)}$, $q = 0, \ldots, Q-1$ of the cyclic channel impulse response which are the time domain representations of the Q channel transfer factors corresponding to the allocated subcarriers. By doing so, the number of unknown elements to be estimated reduces from L_C to Q and the subspace-based semiblind channel estimation is feasible.

In the following, the principle of subspace-based semiblind channel estimation for channels with large delay spread is presented for $U = 1$ user in the system.

The subspace-based semiblind channel estimation is a combination of pilot-assisted channel estimation and subspace-based channel estimation. The pilot-assisted channel estimation is performed by a Least Square (LS) estimation on each pilot carrying subcarrier. The vector containing the LS estimates of the channel transfer factors corresponding to the Q_P pilot carrying subcarriers is calculated by

$$\left[\hat{\tilde{c}}_{\kappa,0}^{(u)}, \ldots, \hat{\tilde{c}}_{\kappa,Q_P-1}^{(u)}\right]^T = \operatorname{diag}\left\{\overline{\boldsymbol{\rho}}^{(u)}\right\}^{-1} \cdot \mathbf{M}_P^{(u)^T} \cdot \mathbf{F}_N \cdot \mathbf{r}_\kappa^{(u)}. \tag{33}$$

For subspace-based channel estimation, the received signal is analyzed before CP removal. As defined in Section 2.3, the vector $\tilde{\mathbf{r}}_k^{(u)}$ includes the received CP part and consists of $LQ = (L_U + L_G)Q$ elements. Due to the IFDMA signal generation by compression, repetition, and phase shifting, it is known that the received vector $\tilde{\mathbf{r}}_k^{(u)}$ comprises L blocks each containing identical data symbols which are compressed in time and phase shifted. Thus, the received vector $\tilde{\mathbf{r}}_k^{(u)}$ can be split into L blocks $\mathbf{r}_{k,j}^{(u)} = [r_{k,jQ}^{(u)}, \ldots, r_{k,jQ+Q-1}^{(u)}]^T$, $j = 0, \ldots, L-1$, each containing the Q transmitted data symbols. The received vector $\tilde{\mathbf{r}}_k^{(u)}$ is represented by L blocks according to

$$\tilde{\mathbf{r}}_k^{(u)} = \left[\mathbf{r}_{k,0}^{(u)}, \ldots, \mathbf{r}_{k,L-1}^{(u)}\right]^T. \tag{34}$$

In the following, three blocks of two neighboring received IFDMA symbols are considered. Due to the assumption that the number L_C of channel delay taps is larger than the number Q of elements per IFDMA block, the last block $\mathbf{r}_{k-1,L-1}^{(u)}$ of the IFDMA symbol with index $k-1$, the first block $\mathbf{r}_{k,0}^{(u)}$ of the CP related to the IFDMA symbol with index k, and the first block $\mathbf{r}_{k,L_G}^{(u)}$ after CP of the IFDMA symbol with index k are influenced by the last L_G blocks of the transmitted IFDMA symbol with index $k-1$ and the first $L_G + 1$ blocks of the transmitted IFDMA symbol with index k as it is illustrated in Figure 5.

Let $\mathbf{H}_{k,0}^{(u)}$ denote the Toeplitz matrix that is given by

$$\mathbf{H}_{k,0}^{(u)} = \begin{bmatrix} h_{k,0}^{(u)} & 0 & \cdots & \cdots & 0 \\ h_{k,1}^{(u)} & h_{k,0}^{(u)} & 0 & \cdots & \vdots \\ \vdots & & \ddots & & 0 \\ h_{k,Q-1}^{(u)} & & \cdots & & h_{k,0}^{(u)} \end{bmatrix}. \tag{35}$$

Further, let $\mathbf{H}_{k,L_G-1}^{(u)}$ and $\mathbf{H}_{k,L_G}^{(u)}$ be defined according to

$$\mathbf{H}_{k,L_G-1}^{(u)} = \begin{bmatrix} h_{k,(L_G-1)Q}^{(u)} & \cdots & & & h_{k,(L_G-2)Q+1}^{(u)} \\ \vdots & \ddots & & & \\ h_{k,L_C-1}^{(u)} & & & & \vdots \\ 0 & \ddots & & \ddots & \\ \vdots & & & & \\ 0 & \cdots & 0 & h_{k,L_C-1}^{(u)} \cdots & h_{k,(L_G-1)Q}^{(u)} \end{bmatrix} \tag{36}$$

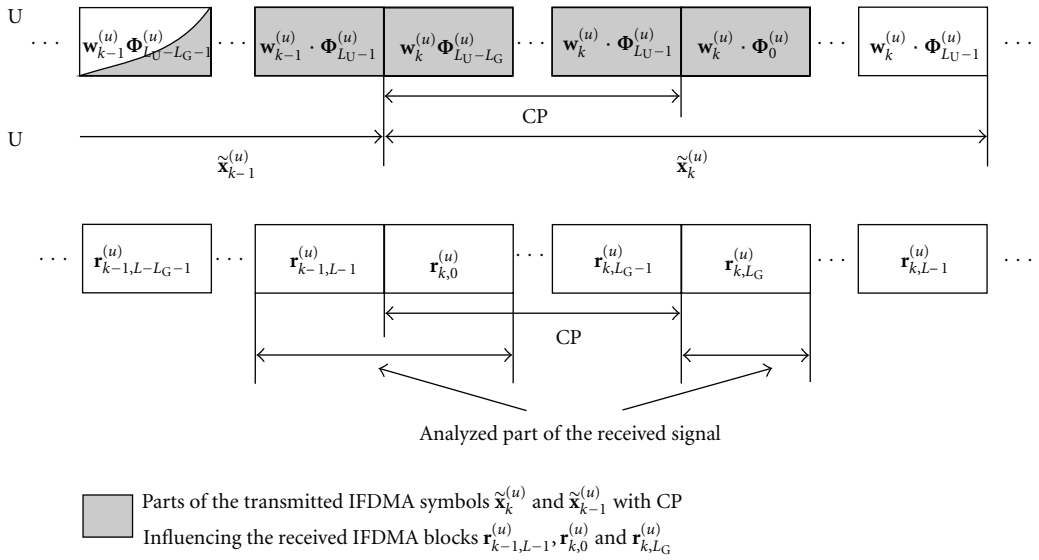

Figure 5: Illustration of the channel influence on the received IFDMA blocks $\mathbf{r}_{k-1,L-1}^{(u)}$, $\mathbf{r}_{k,0}^{(u)}$, and $\mathbf{r}_{k,L_G}^{(u)}$.

$$\mathbf{H}_{k,L_G}^{(u)} = \begin{bmatrix} 0 & \cdots & 0 & h_{k,L_C-1}^{(u)} & \cdots & h_{k,(L_G-1)Q+1}^{(u)} \\ \vdots & & & \ddots & \ddots & \vdots \\ 0 & & \cdots & & 0 & h_{k,L_C-1}^{(u)} \\ 0 & & \cdots & & & 0 \\ \vdots & & & & & \vdots \\ 0 & & \cdots & & & 0 \end{bmatrix}, \quad (37)$$

respectively. The Toeplitz matrices $\mathbf{H}_{k,j}^{(u)}$, $j = 1, \ldots, L_G - 2$, are defined according to

$$\mathbf{H}_{k,j}^{(u)} = \begin{bmatrix} h_{k,jQ}^{(u)} & h_{k,jQ-1}^{(u)} & \cdots & h_{k,(j-1)Q+1}^{(u)} \\ h_{k,jQ+1}^{(u)} & h_{k,jQ}^{(u)} & \cdots & \vdots \\ \vdots & & \ddots & \\ h_{k,(j+1)Q-1}^{(u)} & & \cdots & h_{k,jQ}^{(u)} \end{bmatrix}. \quad (38)$$

Further on, it is assumed that there are only small channel variations in time domain, implying that the matrices $\mathbf{H}_{k,0}^{(u)}$, $\ldots, \mathbf{H}_{k,L_G}^{(u)}$ are approximately constant for the IFDMA symbols with indices $k = 0, \ldots, K-1$, that is,

$$\mathbf{H}_j^{(u)} \approx \mathbf{H}_{k,j}^{(u)}, \quad \text{for } j = 0, \ldots, L_G,\ k = 0, \ldots, K-1. \quad (39)$$

Then, the three received blocks are summarized in a vector that is represented by

$$\begin{bmatrix} \mathbf{r}_{k-1,L-1}^{(u)} \\ \mathbf{r}_{k,0}^{(u)} \\ \mathbf{r}_{k,L_G}^{(u)} \end{bmatrix} = \begin{bmatrix} \mathbf{H}_{L_G}^{(u)} & \cdots & \mathbf{H}_0^{(u)} & \mathbf{0}_Q & \cdots & \mathbf{0}_Q \\ \mathbf{0}_Q & \mathbf{H}_{L_G}^{(u)} & \cdots & \mathbf{H}_0^{(u)} & \cdots & \mathbf{0}_Q \\ \mathbf{0}_Q & \cdots & \mathbf{0}_Q & \mathbf{H}_{L_G}^{(u)} & \cdots & \mathbf{H}_0^{(u)} \end{bmatrix} \cdot \begin{bmatrix} \boldsymbol{\Phi}_{L_U-L_G-1}^{(u)} & \mathbf{0}_Q \\ \vdots & \vdots \\ \boldsymbol{\Phi}_{L_U-1}^{(u)} & \mathbf{0}_Q \\ \mathbf{0}_Q & \boldsymbol{\Phi}_{L_U-L_G}^{(u)} \\ \vdots & \vdots \\ & \boldsymbol{\Phi}_{L_U-1}^{(u)} \\ \mathbf{0}_Q & \boldsymbol{\Phi}_0^{(u)} \end{bmatrix} \cdot \begin{bmatrix} \mathbf{w}_{k-1}^{(u)} \\ \mathbf{w}_k^{(u)} \end{bmatrix} + \begin{bmatrix} \boldsymbol{\nu}_{k-1,L-1}^{(u)} \\ \boldsymbol{\nu}_{k,0}^{(u)} \\ \boldsymbol{\nu}_{k,L_G}^{(u)} \end{bmatrix}. \quad (40)$$

After some calculation of (40), one derives that the inverse

phase-shifted receive vector is equal to

$$\begin{aligned}\begin{bmatrix}\check{\mathbf{r}}_{k-1,L-1}^{(u)}\\ \check{\mathbf{r}}_{k,0}^{(u)}\\ \check{\mathbf{r}}_{k,L_\mathrm{G}}^{(u)}\end{bmatrix} &= \begin{bmatrix}\boldsymbol{\Phi}_{L_\mathrm{U}-1}^{(u)^\mathrm{H}} & \mathbf{0}_Q & \mathbf{0}_Q\\ \mathbf{0}_Q & \boldsymbol{\Phi}_0^{(u)^\mathrm{H}} & \mathbf{0}_Q\\ \mathbf{0}_Q & \mathbf{0}_Q & \boldsymbol{\Phi}_0^{(u)^\mathrm{H}}\end{bmatrix}\cdot\begin{bmatrix}\mathbf{r}_{k-1,L-1}^{(u)}\\ \mathbf{r}_{k,0}^{(u)}\\ \mathbf{r}_{k,L_\mathrm{G}}^{(u)}\end{bmatrix}\\ &= \begin{bmatrix}\mathcal{H}^{(u)}\\ \left(\mathcal{H}^{(u)}-\boldsymbol{\Phi}_0^{(u)^\mathrm{H}}\cdot\mathbf{H}_0^{(u)}\cdot\boldsymbol{\Phi}_0^{(u)}\right)\\ \mathbf{0}_Q\end{bmatrix}\\ &\quad\times\begin{bmatrix}\mathbf{0}_Q\\ \left(\boldsymbol{\Phi}_0^{(u)^\mathrm{H}}\cdot\mathbf{H}_0^{(u)}\cdot\boldsymbol{\Phi}_{L_\mathrm{U}-L_\mathrm{G}}^{(u)}\right)\\ \mathcal{H}^{(u)}\end{bmatrix}\cdot\begin{bmatrix}\mathbf{w}_{k-1}^{(u)}\\ \mathbf{w}_k^{(u)}\end{bmatrix}\\ &\quad+\begin{bmatrix}\boldsymbol{\Phi}_{L_\mathrm{U}-1}^{(u)^\mathrm{H}} & \mathbf{0}_Q & \mathbf{0}_Q\\ \mathbf{0}_Q & \boldsymbol{\Phi}_0^{(u)^\mathrm{H}} & \mathbf{0}_Q\\ \mathbf{0}_Q & \mathbf{0}_Q & \boldsymbol{\Phi}_0^{(u)^\mathrm{H}}\end{bmatrix}\cdot\begin{bmatrix}\boldsymbol{\nu}_{k-1,L-1}^{(u)}\\ \boldsymbol{\nu}_{k,0}^{(u)}\\ \boldsymbol{\nu}_{k,L_\mathrm{G}}^{(u)}\end{bmatrix}.\end{aligned}\tag{41}$$

It can be seen that the system matrix contains the matrices $\mathcal{H}^{(u)}$ (cf. (17)) and $\mathbf{H}_0^{(u)}$ and, thus, the $2Q$ unknown elements $c_0^{(u)},\ldots,c_{Q-1}^{(u)},h_0^{(u)},\ldots,h_{Q-1}^{(u)}$. From the $2Q$ unknown elements, only the Q elements $c_0^{(u)},\ldots,c_{Q-1}^{(u)}$ are necessary to describe the channel influence on the IFDMA received signal and, thus, shall be estimated. With

$$\begin{aligned}\mathbf{H}_\mathrm{sub}^{(u)} &= \begin{bmatrix}\mathcal{H}^{(u)}\\ \left(\mathcal{H}^{(u)}-\boldsymbol{\Phi}_0^{(u)^\mathrm{H}}\cdot\mathbf{H}_0^{(u)}\cdot\boldsymbol{\Phi}_0^{(u)}\right)\\ \mathbf{0}_Q\end{bmatrix}\\ &\quad\times\begin{bmatrix}\mathbf{0}_Q\\ \left(\boldsymbol{\Phi}_0^{(u)^\mathrm{H}}\cdot\mathbf{H}_0^{(u)}\cdot\boldsymbol{\Phi}_{L_\mathrm{U}-L_\mathrm{G}}^{(u)}\right)\\ \mathcal{H}^{(u)}\end{bmatrix},\end{aligned}\tag{42}$$

the autocorrelation matrix of the vector containing the three received blocks is given by

$$\begin{aligned}\boldsymbol{\mathcal{A}}^{(u)} &= \mathrm{E}\left\{\begin{bmatrix}\check{\mathbf{r}}_{k-1,L-1}^{(u)}\\ \check{\mathbf{r}}_{k,0}^{(u)}\\ \check{\mathbf{r}}_{k,L_\mathrm{G}}^{(u)}\end{bmatrix}\cdot\begin{bmatrix}\check{\mathbf{r}}_{k-1,L-1}^{(u)}\\ \check{\mathbf{r}}_{k,0}^{(u)}\\ \check{\mathbf{r}}_{k,L_\mathrm{G}}^{(u)}\end{bmatrix}^\mathrm{H}\right\}\\ &= \mathbf{H}_\mathrm{sub}^{(u)}\cdot\sigma_\mathrm{W}^2\cdot\mathbf{I}_{2Q}\cdot\mathbf{H}_\mathrm{sub}^{(u)^\mathrm{H}}+\sigma_\nu^2\cdot\mathbf{I}_{3Q}.\end{aligned}\tag{43}$$

The first part of the autocorrelation matrix has rank $2Q$ and describes the noise-free case. Thus, the signal subspace is spanned by its eigenvectors which are the columns of the matrix $\mathbf{H}_\mathrm{sub}^{(u)}$ with the signal subspace eigenvalues represented by σ_W^2. The $3Q\times 3Q$ autocorrelation matrix $\boldsymbol{\mathcal{A}}^{(u)}$ is not full rank in the noise-free case. That means that for the noisy case, signal and noise subspace are separable by an eigenvalue decomposition of $\boldsymbol{\mathcal{A}}^{(u)}$ [15]. Assuming the noise power to be smaller than the signal power, the Q eigenvectors corresponding to the Q smallest eigenvalues span the noise subspace. A detailed derivation of the identification of signal and noise subspace can be found in [13] and is not derived in detail in this work. The autocorrelation matrix $\boldsymbol{\mathcal{A}}^{(u)}$ is estimated by the arithmetic mean over K-received IFDMA symbols according to

$$\widehat{\boldsymbol{\mathcal{A}}}^{(u)} = \frac{1}{K}\sum_{k=0}^{K-1}\begin{bmatrix}\check{\mathbf{r}}_{k-1,L-1}^{(u)}\\ \check{\mathbf{r}}_{k,0}^{(u)}\\ \check{\mathbf{r}}_{k,L_\mathrm{G}}^{(u)}\end{bmatrix}\cdot\begin{bmatrix}\check{\mathbf{r}}_{k-1,L-1}^{(u)}\\ \check{\mathbf{r}}_{k,0}^{(u)}\\ \check{\mathbf{r}}_{k,L_\mathrm{G}}^{(u)}\end{bmatrix}^\mathrm{H}.\tag{44}$$

Let $\widehat{\mathbf{g}}_0^{(u)},\ldots,\widehat{\mathbf{g}}_{Q-1}^{(u)}$ denote the eigenvectors corresponding to the Q smallest eigenvalues of the matrix $\widehat{\mathcal{A}}^{(u)}$ that span the noise subspace. Then, the orthogonality constraint

$$\widehat{\mathbf{g}}_q^{(u)^\mathrm{H}}\cdot\mathbf{H}_\mathrm{sub}^{(u)} = \mathbf{0}_{1\times 2Q}\quad\text{for } q=0,\ldots,Q-1\tag{45}$$

must hold as signal and noise subspace are orthogonal to each other [15].

In the following, the elements $c_0^{(u)},\ldots,c_{Q-1}^{(u)}$ will be estimated. Necessarily, the estimation of the elements $h_q^{(u)}$, $q=0,\ldots,Q-1$, is also required as the system matrix depends inevitably on these elements. Then, the desired elements $c_q^{(u)}$, $q=0,\ldots,Q-1$, are estimated via the estimation of the vector $[c_0^{(u)},\ldots,c_{Q-1}^{(u)},h_0^{(u)},\ldots,h_{Q-1}^{(u)}]^\mathrm{T}$ containing the desired and the undesired elements. For the estimation, the noise subspace eigenvectors $\widehat{\mathbf{g}}_q^{(u)}$, $q=0,\ldots,Q-1$, are transformed into the $2Q\times 2Q$ matrices $\widehat{\mathcal{G}}_q^{(u)}$, $q=0,\ldots,Q-1$ as explained in the Appendix. Then, the orthogonality constraint can be given in dependency of the vector $[c_0^{(u)},\ldots,c_{Q-1}^{(u)},h_0^{(u)},\ldots,h_{Q-1}^{(u)}]^\mathrm{T}$ by

$$\left[c_0^{(u)},\ldots,c_{Q-1}^{(u)},h_0^{(u)},\ldots,h_{Q-1}^{(u)}\right]^*\cdot\widehat{\mathcal{G}}_q^{(u)} = \mathbf{0}_{1\times 2Q}.\tag{46}$$

The vector $[c_0^{(u)},\ldots,c_{Q-1}^{(u)},h_0^{(u)},\ldots,h_{Q-1}^{(u)}]^\mathrm{T}$ can additionally be represented in dependency of the vector $[\widehat{\bar{c}}_{\kappa,0}^{(u)},\ldots,\widehat{\bar{c}}_{\kappa,Q_\mathrm{P}-1}^{(u)}]^\mathrm{T}$ containing the pilot-assisted channel estimates. Let

$$\widetilde{\boldsymbol{\mathcal{F}}} = [\boldsymbol{\mathcal{F}}\,\mathbf{0}_{Q_\mathrm{P}\times Q}]\tag{47}$$

denote a $Q_\mathrm{P}\times 2Q$ matrix containing the $Q_\mathrm{P}\times Q$ matrix $\boldsymbol{\mathcal{F}}$ and zero elements. Then, the relation

$$\widetilde{\boldsymbol{\mathcal{F}}}\cdot\left[c_0^{(u)},\ldots,c_{Q-1}^{(u)},h_0^{(u)},\ldots,h_{Q-1}^{(u)}\right]^\mathrm{T} = \left[\widehat{\bar{c}}_{\kappa,0}^{(u)},\ldots,\widehat{\bar{c}}_{\kappa,Q_\mathrm{P}-1}^{(u)}\right]^\mathrm{T}\tag{48}$$

is valid for the pilot-assisted channel estimates.

As explained in [13], Equations (46) and (48) are combined in a system of equations and an estimate $[\hat{c}_0^{(u)},\ldots,\hat{c}_{Q-1}^{(u)},\hat{h}_0^{(u)},\ldots,\hat{h}_{Q-1}^{(u)}]^\mathrm{T}$ is found by minimizing the function

$$\begin{aligned}&\sum_{q=0}^{Q-1}\left\|\left[c_0^{(u)},\ldots,c_{Q-1}^{(u)},h_0^{(u)},\ldots,h_{Q-1}^{(u)}\right]^*\cdot\widehat{\mathcal{G}}_q^{(u)}\right\|_2^2\\ &\quad+\left\|\widetilde{\boldsymbol{\mathcal{F}}}\cdot\left[c_0^{(u)},\ldots,c_{Q-1}^{(u)},h_0^{(u)},\ldots,h_{Q-1}^{(u)}\right]^\mathrm{T}\right.\\ &\quad\left.-\left[\widehat{\bar{c}}_{\kappa,0}^{(u)},\ldots,\widehat{\bar{c}}_{\kappa,Q_\mathrm{P}-1}^{(u)}\right]^\mathrm{T}\right\|_2^2.\end{aligned}\tag{49}$$

The solution is calculated according to [13] and the estimate results in

$$\left[\hat{c}_0^{(u)},\ldots,\hat{c}_{Q-1}^{(u)},\hat{h}_0^{(u)},\ldots,\hat{h}_{Q-1}^{(u)}\right]^{\mathrm{T}} = \left(\sum_{q=0}^{Q-1}\hat{\boldsymbol{\mathcal{G}}}_q^{(u)}\cdot\hat{\boldsymbol{\mathcal{G}}}_q^{(u)^{\mathrm{H}}}+\widetilde{\boldsymbol{\mathcal{F}}}^{\mathrm{H}}\cdot\widetilde{\boldsymbol{\mathcal{F}}}\right)^{-1} \cdot\widetilde{\boldsymbol{\mathcal{F}}}^{\mathrm{H}}\cdot\left[\hat{\tilde{c}}_{\kappa,0}^{(u)},\ldots,\hat{\tilde{c}}_{\kappa,Q_{\mathrm{P}}-1}^{(u)}\right]^{\mathrm{T}}. \tag{50}$$

The subspace-based semiblind channel estimate vector $[\hat{c}_0^{(u)},\ldots,\hat{c}_{Q-1}^{(u)},\hat{h}_0^{(u)},\ldots,\hat{h}_{Q-1}^{(u)}]^{\mathrm{T}}$ is based on the estimate of the autocorrelation matrix via the arithmetic mean in (44) and, therefore, it represents a joint estimate for all IFDMA symbols with indices $k = 0,\ldots,K-1$. For equalization purposes, only the first Q elements $\hat{c}_q^{(\mathrm{u})}$, $q = 0,\ldots,Q-1$, of the estimated vector are necessary and the elements $\hat{h}_0^{(u)},\ldots,\hat{h}_{Q-1}^{(u)}$ are disregarded. The application of the $Q\times Q$ DFT matrix $\mathbf{F}_{\mathrm{Q}}$ to the vector $[\hat{c}_0^{(u)},\ldots,\hat{c}_{Q-1}^{(u)}]^{\mathrm{T}}$ leads to the vector $\hat{\tilde{\mathbf{c}}}^{(u)}$ containing the estimates for each allocated subcarrier which are valid for the IFDMA symbols with indices $k = 0,\ldots,K-1$ and are obtained by

$$\hat{\tilde{\mathbf{c}}}^{(u)} = \mathbf{F}_{\mathrm{Q}}\cdot\left[\hat{c}_0^{(u)},\ldots,\hat{c}_{Q-1}^{(u)}\right]^{\mathrm{T}}. \tag{51}$$

4.2. Estimation of Time Domain Channel Variations. In this section, the proposed subspace-based semiblind channel estimation is combined with decision-directed channel estimation according to our work previously presented in [18]. The subspace-based semiblind channel estimate derived in Section 4.1 represents a joint estimate for each IFDMA symbol within the TDMA slot as the channel variations within the TDMA slot have assumed to be negligible for the derivation of the algorithm. Nevertheless, time varying channel conditions will be considered in the following and, therefore, decision-directed channel estimation is applied in order to estimate the channel variations in time domain.

In [27, 28], decision-directed channel estimation has been presented for IFDMA. In [29], decision-directed channel estimation is proposed for the general case of single carrier systems and a two times one-dimensional Wiener interpolation filter is applied to refine the final decision-directed channel estimate. For IFDMA, the application of these decision-directed channel estimation algorithms leads to high error propagation. Thus, in the following, we consider a decision-directed channel estimation algorithm which aims at minimizing the error propagation with the help of an iterative Wiener filtering within each estimation step that is applied jointly to the decision-directed channel estimates corresponding to a certain number of neighboring IFDMA symbols. The filtered update estimates are used iteratively for the decision-directed channel estimation again. The considered algorithm will be denoted by Decision-directed Channel Estimation with iterative Wiener Filtering (DDCE + WF) in the following. For the application of DDCE + WF, one pilot carrying IFDMA symbol within the total number K of transmitted IFDMA symbols is required to estimate the channel variations in time domain. Based on the pilot symbols that are transmitted within the pilot carrying IFDMA symbol, the subspace-based semiblind channel estimation can be applied according to Section 4.1. By this means, the vector $\hat{\tilde{\mathbf{c}}}^{(u)}$ can be obtained which contains the estimates $\hat{\tilde{c}}_0^{(u)},\ldots,\hat{\tilde{c}}_{Q-1}^{(u)}$ of the channel transfer factors corresponding to the Q-allocated subcarriers which are valid for the IFDMA symbols with indices $k = 0,\ldots,K-1$. These estimates are utilized for the initialization of the DDCE + WF by setting $\tilde{\tilde{\mathbf{c}}}_0^{(u)} = \hat{\tilde{\mathbf{c}}}^{(u)}$. The initialization of the algorithm comprises the equalization of the received IFDMA symbols with the estimates $\hat{\tilde{c}}_0^{(u)},\ldots,\hat{\tilde{c}}_{Q-1}^{(u)}$. The equalized IFDMA symbols are deinterleaved, decoded, and demapped in order to get an estimate for the transmitted data bits. Subsequently, the estimated data bits are mapped onto data symbols, interleaved and coded, again, and utilized to get an update estimate of the channel transfer factors. These update estimates are fed into a Wiener filter with V coefficients in order to obtain the filtered update estimates. With the filtered update estimates, the data symbols are estimated again. The procedure is performed K-times, that is, for each IFDMA symbol within the TDMA slot.

Let e_1, e_2, and e_3 denote indices that are defined according to

$$e_1 = \begin{cases} V, & \text{for } k \le \dfrac{V}{2},\\ K-1, & \text{for } k > K-\dfrac{V}{2}-1,\\ k+\dfrac{V}{2}-1, & \text{else,}\end{cases}$$

$$e_2 = \begin{cases} k-V, & \text{for } k \le \dfrac{V}{2},\\ k+1-K, & \text{for } k > K-\dfrac{V}{2}-1,\\ -\dfrac{V}{2}+1, & \text{else,}\end{cases} \tag{52}$$

$$e_3 = \begin{cases} k-1, & \text{for } k \le \dfrac{V}{2},\\ V-K+k, & \text{for } k > K-\dfrac{V}{2}-1,\\ \dfrac{V}{2}, & \text{else,}\end{cases}$$

respectively.

Then, the iterative procedure of the DDCE + WF is presented in Algorithm 1. The Wiener filter coefficients a_v with $v = e_2,\ldots,0,\ldots,e_3$ are derived such that $\mathrm{E}\{|\tilde{\tilde{\mathbf{c}}}_k^{(u)} - \overline{\mathbf{c}}_k^{(u)}|\}$ becomes minimum. A detailed derivation of Wiener filter coefficients can be found in, for example, [30] and is not presented in this work.

5. Performance Analysis

5.1. Mean Square Error. In this section, the presented semiblind channel estimation is investigated with regard to

(1) Initialization

Equalization with $\hat{\tilde{\mathbf{c}}}^{(u)} = [\hat{c}_0^{(u)}, \ldots, \hat{c}_{Q-1}^{(u)}]^{\mathrm{T}}$

Estimation of the IFDMA symbols: $\hat{\mathbf{d}}_1^{(u,0)}, \ldots, \hat{\mathbf{d}}_V^{(u,0)}$

Frequency domain representation: $\hat{\overline{\mathbf{d}}}_1^{(u,0)}, \ldots, \hat{\overline{\mathbf{d}}}_V^{(u,0)}$

Initialize: $\tilde{\overline{\mathbf{c}}}_0^{(u)} = \hat{\overline{\mathbf{c}}}^{(u)}$

For $k = 1, \ldots, K-1$

(2) Decision-directed channel estimation

$$\hat{\overline{\mathbf{c}}}_k^{(u,k)} = \frac{\overline{\mathbf{y}}_k^{(u)}}{\hat{\overline{\mathbf{d}}}_k^{(u,k-1)}}, \ldots, \hat{\overline{\mathbf{c}}}_{e_1}^{(u,k)} = \frac{\overline{\mathbf{y}}_{e_1}^{(u)}}{\hat{\overline{\mathbf{d}}}_{e_1}^{(u,k-1)}}$$

(3) Wiener filtering with V filter coefficients

$$\tilde{\overline{\mathbf{c}}}_k^{(u)} = \sum_{v=e_2}^{0} a_v \cdot \hat{\overline{\mathbf{c}}}_{k-v}^{(u,k)} + \sum_{v=1}^{e_3} a_v \cdot \tilde{\overline{\mathbf{c}}}_{k-v}^{(u)}$$

(4) Equalization with $\tilde{\overline{\mathbf{c}}}_{\mathbf{k}}^{(\mathbf{u})}$

Estimation of the IFDMA symbols: $\hat{\mathbf{d}}_{k+1}^{(u,k)}, \ldots, \hat{\mathbf{d}}_{e_1}^{(u,k)}$

Frequency domain representation: $\hat{\overline{\mathbf{d}}}_{k+1}^{(u,k)}, \ldots, \hat{\overline{\mathbf{d}}}_{e_1}^{(u,k)}$

end

Algorithm 1: Decision-directed channel estimation with iterative wiener filtering.

the Mean Square Error (MSE) performance. The MSE is defined as

$$\mathrm{MSE} = \frac{1}{K} \sum_{k=0}^{K-1} \frac{\left\| \hat{\overline{\mathbf{c}}}_k^{(u)} - \overline{\mathbf{c}}_k^{(u)} \right\|_2^2}{\left\| \overline{\mathbf{c}}_k^{(u)} \right\|_2^2}. \tag{53}$$

The results are obtained by computer simulations and are valid for the parameters presented in Table 2. Besides the WINNER SCM urban macrocell channel, a second channel model is used for the simulations. Here, the time variant multipath channel is modeled by L_C-independent Rayleigh-fading coefficients that exhibit a decaying power with the delay time τ according to the delay power spectral density for typical urban channels or rural area channels defined in the European working group COST 207 [31]. This second channel model is utilized because the channel estimation performance will be investigated for different numbers L_C of channel delay taps. The usage of this second channel model allows a variable adjustment of the parameter L_C and, thus, this channel model will be referred to as Typical Urban VarDelay channel or Rural Area VarDelay channel in the following.

In the following, the MSE is given as a function of E_B/N_0 in dB. The results are obtained by transmitting $Q_P = Q/2$ pilot symbols in the IFDMA symbol with index $k = 0$ which corresponds to an interpolation depth $I = 2$ meaning that every second subcarrier in the IFDMA symbol with index $k = 0$ is used for pilot transmission. As the new semiblind channel estimation approach will support a reduction of the number of pilot carrying subcarriers even for a large number L_C of channel delay taps compared to the parameter Q, the following results are presented for $Q = 8$ and $K = 30$.

In Figure 6(a), the influence of the number L_C of channel delay taps on the estimation performance of the subspace-based semiblind channel estimation is investigated for the Typical Urban VarDelay channel. In order to observe the influence of channel delay spread independently from time varying channel conditions, the results are presented for a user velocity $v = 0$ km/h. For subspace-based semiblind channel estimation, the results in Figure 6(a) are obtained by applying the algorithm introduced in [18] for $L_C = Q$ and the algorithm introduced in this paper for $L_C > Q$. In order to fulfill the sampling theorem in frequency domain, an interpolation depth $I = 1$ had to be applied meaning that each allocated subcarrier had to be used for pilot transmission. Thus, the presented results are valid for a two times extended sampling theorem in frequency domain as only every second subcarrier is used for pilot transmission.

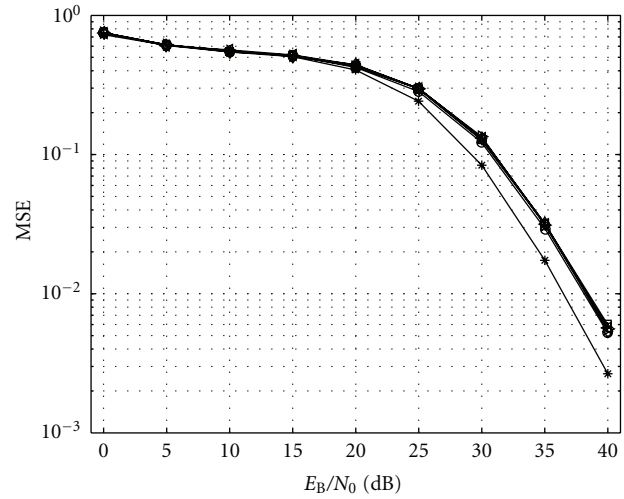

(a) Typical Urban VarDelay channel

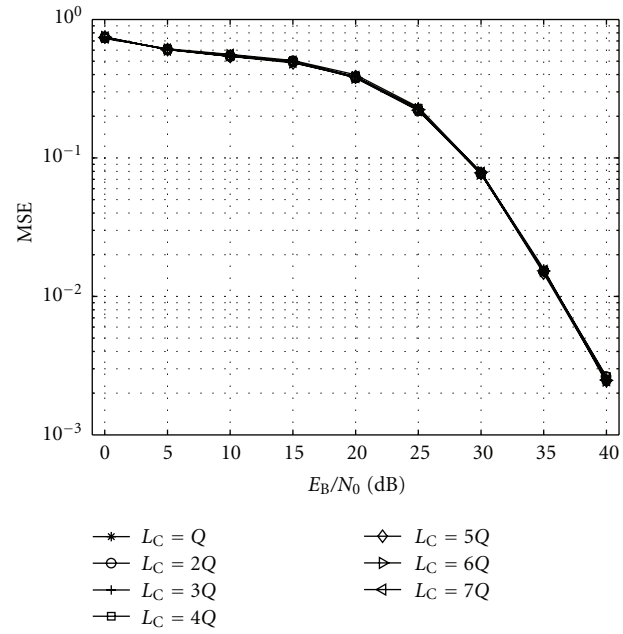

(b) Rural Area VarDelay channel

Figure 6: MSE as a function of E_B/N_0 with the number L_C of channel delay taps as parameter for (a) Typical Urban VarDelay and (b) Rural Area VarDelay channel assuming that $Q = 8$, $K = 30$, $U = 1$, $v = 0$ km/h, and $I = 2$.

Table 2: System and channel parameters.

System parameters	
Carrier frequency	$f_0 = 3.7\,\text{GHz}$
Bandwidth	$B = 40\,\text{MHz}$
Number of subcarriers	$N = 1024$
Modulation	QPSK
Coding	Convolutional coding
Code rate	1/2
Constraint length	6
Decoder	Max-Log-MAP [32, 33]
Equalizer	Linear MMSE FDE [34]
Interleaving	Random
Interleaving depth	0.8 ms
Guard interval duration	$T_G = 3.2\,\mu\text{s}$
Number K of IFDMA symbols per TDMA slot	$K = 30$
Channel parameters	
Channel	WINNER SCM [35]
Channel scenario	urban macrocell
Coherence bandwidth	$B_{\text{coh}} \approx 290\,\text{kHz}$
Channel	VarDelay
Channel scenario	typical urban/rural area [31]

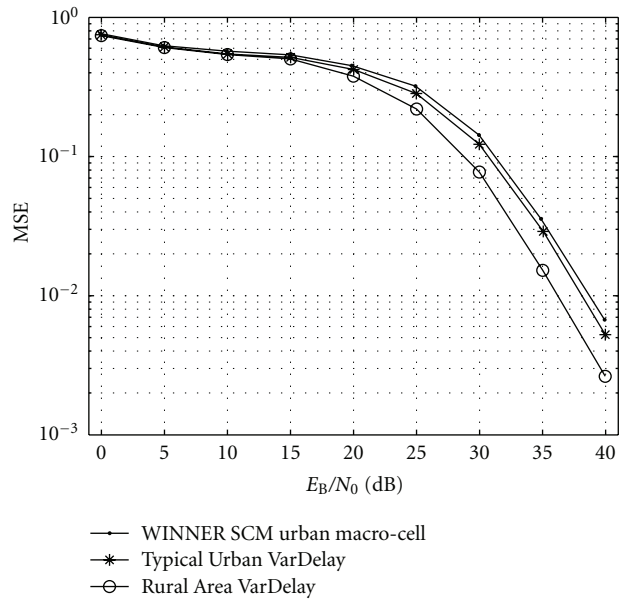

Figure 7: MSE as a function of E_B/N_0 with the considered channel model as parameter assuming that $Q = 8$, $K = 30$, $U = 1$, $v = 0\,\text{km/h}$, and $I = 2$.

It can be seen that the estimation of channels with $L_C > Q$ for subspace-based semiblind channel estimation leads to a slightly increased MSE compared to the estimation for $L_C = Q$. The increase of the MSE can be reduced to the fact that for $L_C > Q$, $2Q$ unknown elements comprising the first Q elements of the channel impulse response and the Q elements of the cyclic channel impulse response have to be estimated instead of Q unknowns for the case where $L_C = Q$. For $L_C > Q$, the MSE is independent of the specific value for L_C and, thus, it can be stated that due to estimating the cyclic channel impulse response according to the algorithm presented in Section 4.1 the estimation performance is independent of the channel delay spread.

The results in Figure 6(b) are valid for the same assumptions as in Figure 6(a), but for the Rural Area VarDelay channel. It can be seen that there is no performance degradation for the case where $L_C > Q$ compared to $L_C = Q$. This can be explained by the power distribution of channel delay taps for the case of a rural area propagation scenario. The amount of power that is accumulated in the first channel delay taps is larger than for the typical urban propagation scenario. As the subspace-based semiblind channel estimation takes advantage of the interference that is introduced by the preceding IFDMA symbol into the CP of the current IFDMA symbol, the algorithm performs better if a larger amount of power is accumulated in the first channel delay taps.

In the following, the influence of the considered channel model on the estimation performance of the subspace-based semiblind channel estimation is investigated for the case of channels with large delay spreads. In Figure 7, the MSE is given as a function of E_B/N_0 in dB with the considered channel model as parameter. For comparison, the WINNER SCM urban macrocell channel, the Typical Urban VarDelay channel, and the Rural Area VarDelay channel are investigated. The results are again presented for a user velocity $v = 0\,\text{km/h}$. It can be seen that the subspace-based semiblind channel estimation performs best in case of the rural area propagation scenario. This can be deduced to the fact that a large amount of the total power of the channel delay paths is accumulated in the first delay taps. The comparison between the WINNER SCM urban macrocell channel, and the Typical Urban VarDelay channel shows that the subspace-based semiblind channel estimation copes slightly better with the Typical Urban VarDelay channel. Although there is only slight difference in the MSE performance, it can be deduced that the subspace-based semiblind channel estimation performs better in case of a continuously decaying power delay profile.

In Figure 8(a), the performance of the proposed DDCE + WF with subspace-based semiblind channel estimation as initialization is investigated. The MSE is given as a function of E_B/N_0 in dB with the user velocity v as parameter. For the simulation, the WINNER SCM urban macrocell channel is used and $Q_P = Q/2$ pilot symbols are transmitted in the IFDMA symbol with index $k = 0$. The pilot symbols are inserted according to an interpolation depth $I = 2$ which leads to a distance of $256 \cdot \Delta f$ between neighboring pilot carrying subcarriers. For the iterative Wiener filtering, $V = 6$ filter coefficients are applied.

It can be seen that the performance of DDCE + WF with subspace-based semiblind channel estimation as initialization exhibits a satisfying performance. Comparing the result for $v = 0\,\text{km/h}$ with the result for subspace-based semiblind channel estimation shown in Figure 7, it reveals that the application of DDCE + WF considerably

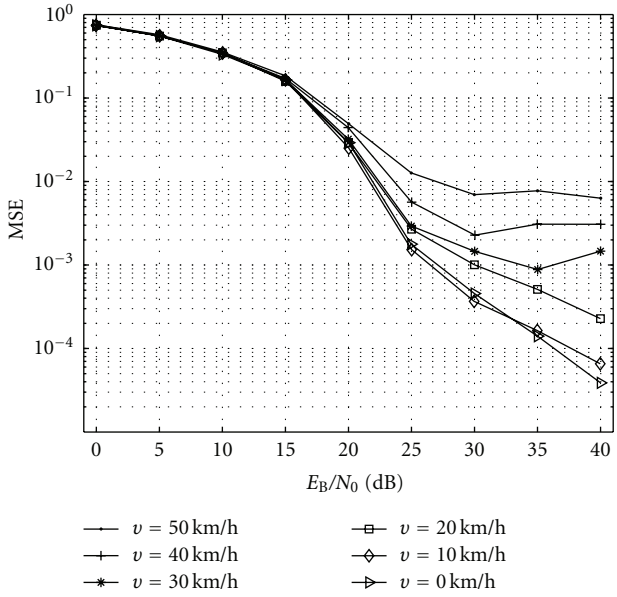

(a) Comparison of correlation and subspace-based semiblind channel estimation with interpolation depth $I = 2$ as initialization for DDCE + WF

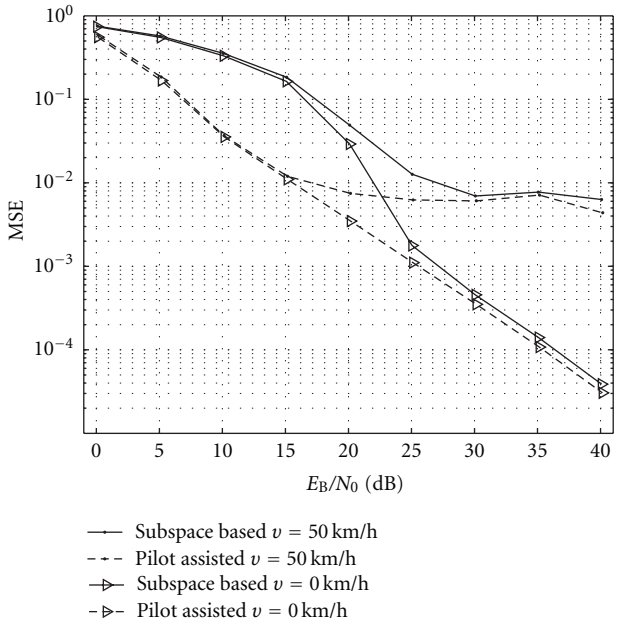

(b) Comparison of subspace-based semiblind channel estimation with interpolation depth $I = 2$ and pilot-assisted channel estimation with $I = 1$ as initialization for DDCE + WF

FIGURE 8: MSE as a function of E_B/N_0 with the velocity v as parameter for the WINNER SCM urban macrocell channel and assuming that $Q = 8$, $K = 30$, and $U = 1$.

improves the estimation performance. For an example, the improvement is approximately 15 dB at a given mse of MSE $= 10^{-2}$. This shows that the application of DDCE + WF for the estimation of time domain channel variations mitigates estimation errors that occur due to an erroneous estimation of the frequency domain channel variations. Due to symbol detection, updating channel estimation, and subsequent Wiener filtering in each iteration step for DDCE + WF, the propagation of the estimation error caused by the initializing estimate is strongly mitigated. As the performance improvement of DDCE + WF increases for increasing Signal-to-Noise Ratio (SNR) values, it can be deduced that the proposed DDCE + WF requires a certain quality of its initializing estimate to develop its error mitigating property. Obviously, for low SNR values, the estimation performance is insufficient and cannot be improved noticeably by the application of DDCE + WF. On the contrary, for $E_B/N_0 > 5$ dB, the initializing estimate provides a satisfying performance and, thus, the performance can be improved significantly. Nevertheless, for increasing velocities v, the MSE of DDCE + WF with subspace-based semiblind channel estimation as initialization exhibits an increasing error floor for large SNR values. The increasing error floor can be explained by an error propagation due to the time varying channel conditions. The error propagation is reduced by the iterative Wiener filtering but cannot be completely avoided.

In Figure 8(b), the performance of the proposed DDCE + WF with subspace-based semiblind channel estimation as initialization is compared to the case where pure pilot-assisted channel estimation with LS estimation for each allocated subcarrier is used for the initialization of the DDCE + WF. The results in Figure 8(b) are valid for the same assumptions as in Figure 8(a). As the pure pilot-assisted initialization consumes twice as much pilot symbols as the subspace-based semiblind initialization, the pilot symbol overhead is included in the MSE results as an SNR degradation according to [9].

Figure 8(b) shows that for $E_B/N_0 < 25$ dB, the DDCE + WF with pure pilot-assisted initialization exhibits a clear better performance than the DDCE + WF with subspace-based semiblind initialization. This can be attributed to the fact that the pilot-assisted channel estimation provides better estimation performances for $E_B/N_0 < 25$ dB than the subspace-based semiblind channel estimation. The high quality of the pilot-assisted initializing estimate leads to a strong performance improvement while applying DDCE + WF. Nevertheless, for $E_B/N_0 \geq 25$ dB, the DDCE + WF with subspace-based semiblind initialization exhibits the same performance as DDCE + WF with pilot-assisted initialization. This result is remarkable as the subspace-based initializing estimate requires half the number of pilot symbols than the pilot-assisted initializing estimate and provides satisfying estimation performance for a pilot allocation where the pilot-assisted initialization fails to estimate the channel at all. Moreover, it can be stated that the performance gain due to the application of DDCE + WF is significantly larger for the subspace-based semiblind initialization than for the pilot-assisted initialization.

5.2. Complexity. In this section, the proposed channel estimation algorithm is investigated in terms of computational complexity. The computational complexity is measured based on the required number of complex multiplications

which are calculated and compared for the DDCE + WF with semiblind subspace-based initialization and the DDCE + WF with pure pilot-assisted initialization. In the following, divisions are assumed to have the same computational complexity as multiplications and repeated operations are assumed to contribute only once to the computational complexity as the result of these operations can be stored and reused. Further on, the calculation of the Wiener filter coefficients can be realized once in an offline process and the result can be stored in memory and retrieved for the filtering operations. Therefore, the calculation of the Wiener filter coefficients is discounted within the complexity considerations and only the filtering operations themselves are counted. In Table 3, the number of complex multiplications is given for the respective estimation algorithm. It is assumed that the $Q\times Q$ DFT and IDFT operations can be implemented by Fast Fourier Transform (FFT) and Inverse Fast Fourier Transform (IFFT) operations according to [36] with $Q \cdot \log_2(Q)$ complex multiplications each.

For both algorithms, the second line given by $K \cdot (Q \cdot (V + 2) + 2 \cdot Q \cdot \log_2(Q) + \mathcal{O}(\text{decoding}))$ is identical as it refers to the number of complex multiplications for the DDCE + WF. In each of the $K - 1$ iteration steps, there are $2 \cdot Q \cdot \log_2(Q)$ multiplications for the FFT and IFFT operations applied to the estimated data symbols, Q multiplications for the LS estimation, Q multiplication for the equalization, and $V \cdot Q$ multiplications for the Wiener filtering. The multiplications for the coding and decoding process in each iteration step are neglected at this point, as the coding and decoding processes do not represent the crucial part of the algorithms in terms of complexity. The number of multiplications strongly depends on the coding and decoding algorithms and their implementation and, thus, varies for different coding and decoding algorithms. For subspace-based semiblind initialization, there are Q_P multiplications for the LS estimates of the pilot carrying subcarriers. The calculation of the $3Q \times 3Q$ autocorrelation matrix consumes $L_\mathrm{U} \cdot K \cdot (3 \cdot Q)^2$ multiplications. The complexity order of the eigenvalue decomposition of an $L \times L$ matrix has been presented in, for example, [26] and equals $\mathcal{O}(5/3L^3)$. For $L = 3Q$, the eigenvalue decomposition of the $3Q \times 3Q$ autocorrelation matrix entails a large number of complex multiplications and leads to a complexity order $\mathcal{O}(45\ Q^3)$. Finally, the calculation of (50) utilizes $8 \cdot Q^4 + 2 \cdot Q^2 + Q \cdot Q_\mathrm{P}$ multiplications and the FFT operation in order to obtain the channel transfer factors utilizes $Q \cdot \log_2(Q)$ multiplications. For the subspace-based semiblind initialization, the critical part in terms of complexity is the computation of $\sum_{q=0}^{Q-1} \hat{\mathbf{g}}_q^{(u)} \cdot \hat{\mathbf{g}}_q^{(u)\mathrm{H}}$ which leads to $8Q^4$ complex multiplications.

The initialization of DDCE + WF with pure pilot-assisted channel estimation utilizes only Q multiplications for the LS estimates of the Q pilot carrying subcarriers. It can be stated that initialization with pilot-assisted channel estimation exhibits a clearly lower computational complexity than initialization with the subspace-based semiblind channel estimation.

6. Conclusion

It has been shown that the number of unknowns that shall be estimated by subspace-based semiblind channel estimation to describe the influence of the channel on each received IFDMA symbol can be reduced to the number Q of allocated subcarriers. For IFDMA, the introduced subspace-based semiblind channel estimation is able to estimate the Q channel transfer factors corresponding to the subcarriers allocated to a certain user even if the sampling theorem in frequency domain is not fulfilled by the insertion of pilot symbols and the delay spread of the channel is large. The new algorithm provides comparable performance as the previously introduced algorithm for channels with small delay spreads. The combination of the proposed subspace-based semiblind channel estimation with the DDCE + WF allows the reduction of the pilot symbol overhead in frequency and compared to pure pilot-assisted channel estimation as the sampling theorem in frequency and time domain can be violated. The combination of the new subspace-based semiblind estimation with the proposed DDCE + WF is advantageous in terms of an improved estimation performance due to the iterative Wiener filtering. The initialization of the DDCE + WF with the introduced subspace-based semiblind initialization provides comparable performance to the initialization with pure pilot-assisted channel estimation for large SNR. In this work, channel estimation with a reduced number of pilot symbols has been successfully completed for IFDMA in case of low to moderate velocities of the mobile terminal. For high-mobility channels, the difficulty of convergence arises for the autocorrelation matrix estimation and the presented algorithm can only provide unsatisfactory estimation performance. As future work, the IFDMA characteristic signal structure will be further exploited in order to achieve an improved and faster converging estimation of the autocorrelation matrix. By this means the presented algorithm will be applicable to higher-mobility channels and provide reliable channel estimation performance in this case.

Appendix

In the following, the transformation of the noise subspace eigenvectors $\hat{\mathbf{g}}_q^{(u)}$ into the matrices $\hat{\mathbf{G}}_q^{(u)}$ for $q = 0, \ldots, Q-1$ is explained for the algorithm presented in Section 4. The derivation is based on [13] and adapted to the application to IFDMA channel estimation. The matrices $\hat{\mathbf{G}}_q^{(u)}$ are utilized to represent (45) explicitly as a function of the $1 \times 2Q$ vector $[c_0^{(u)}, \ldots, c_{Q-1}^{(u)}, h_0^{(u)}, \ldots, h_{Q-1}^{(u)}]^*$.

The $3Q \times 1$ vector $\mathbf{g}_q^{(u)}$ is split up in three $Q \times 1$ vectors $\mathbf{g}_{q,j}^{(u)}$, $j = 0, 1, 2$. With $[\mathbf{g}_q^{(u)}]_q$ denoting the qth element of $\mathbf{g}_q^{(u)}$, the vectors $\mathbf{g}_{q,j}^{(u)}$, $j = 0, 1, 2$ are defined according to

$$\mathbf{g}_{q,j}^{(u)} = \left[\left[\mathbf{g}_q^{(u)}\right]_{jQ}, \ldots, \left[\mathbf{g}_q^{(u)}\right]_{jQ+Q-1}\right]^\mathrm{T}. \tag{A.1}$$

Table 3: Number of complex multiplications.

Algorithm	Complex multiplications
Pilot-assisted channel estimation + DDCE + WF	$Q + (K-1)\cdot(Q\cdot(V+2)+2\cdot Q\cdot\log_2(Q))$
Subspace-based semiblind channel estimation + DDCE + WF	$8Q^4+\mathcal{O}(45Q^3)+(9L_{\mathrm{U}}K+2)\cdot Q^2+(Q_{\mathrm{P}}+\log_2(Q))\,Q+Q_{\mathrm{P}}$ $+(K-1)\cdot(Q\cdot(V+2)+2\cdot Q\cdot\log_2(Q))$

With this, (45) can be rewritten according to

$$\begin{aligned}\hat{\mathbf{g}}_q^{(u)\mathrm{H}}\cdot\Bigg[&\begin{pmatrix}\mathcal{H}^{(u)}\\ \left(\mathcal{H}^{(u)}-\boldsymbol{\Phi}_0^{(u)\mathrm{H}}\cdot\mathbf{H}_0^{(u)}\cdot\boldsymbol{\Phi}_0^{(u)}\right)\\ \mathbf{0}_Q\end{pmatrix}\\ &\times\begin{pmatrix}\mathbf{0}_Q\\ \boldsymbol{\Phi}_0^{(u)\mathrm{H}}\cdot\mathbf{H}_0^{(u)}\cdot\boldsymbol{\Phi}_{L_U-L_G}^{(u)}\\ \mathcal{H}^{(u)}\end{pmatrix}\Bigg]\\ =\Big[&\hat{\mathbf{g}}_{q,0}^{(u)\mathrm{H}}\cdot\mathcal{H}^{(u)}+\hat{\mathbf{g}}_{q,1}^{(u)\mathrm{H}}\cdot\mathcal{H}^{(u)}-\hat{\mathbf{g}}_{q,1}^{(u)\mathrm{H}}\cdot\boldsymbol{\Phi}_0^{(u)\mathrm{H}}\cdot\mathbf{H}_0^{(u)}\\ &\cdot\boldsymbol{\Phi}_0^{(u)},\hat{\mathbf{g}}_{q,1}^{(u)\mathrm{H}}\cdot\boldsymbol{\Phi}_0^{(u)\mathrm{H}}\cdot\mathbf{H}_0^{(u)}\cdot\boldsymbol{\Phi}_{L_U-L_G}^{(u)}+\hat{\mathbf{g}}_{q,2}^{(u)\mathrm{H}}\cdot\mathcal{H}^{(u)}\Big].\end{aligned}\tag{A.2}$$

Let $\mathbf{C}_{q,j}^{(u)}$ denote a $2Q\times Q$ matrix that is defined by

$$\begin{aligned}&\mathbf{C}_{q,j}^{(u)}\\ &=\begin{bmatrix}0&\cdots&0\\ \vdots&\cdots&\vdots\\ 0&\cdots&0\\ \left[\hat{\mathbf{g}}_{q,j}^{(u)}\right]_0\cdot e^{j0\varphi^{(u)}}&\cdots&\left[\hat{\mathbf{g}}_{q,j}^{(u)}\right]_{Q-1}\cdot e^{j(Q-1)\varphi^{(u)}}\\ \vdots&&0\\ \vdots&\iddots&\vdots\\ \left[\hat{\mathbf{g}}_{q,j}^{(u)}\right]_{Q-1}\cdot e^{j(Q-1)\varphi^{(u)}}&0\quad\cdots&0\end{bmatrix}\\ &\cdot\boldsymbol{\Phi}_0^{(u)},\end{aligned}\tag{A.3}$$

Further, let $\mathbf{D}_{q,j}^{(u)}$ denote a $2Q\times Q$ matrix that is defined by

$$\mathbf{D}_{q,j}^{(u)}=\begin{bmatrix}\left[\hat{\mathbf{g}}_{q,j}^{(u)}\right]_0&\left[\hat{\mathbf{g}}_{q,j}^{(u)}\right]_1&\cdots&\left[\hat{\mathbf{g}}_{q,j}^{(u)}\right]_{Q-1}\\ \vdots&&\iddots&\left[\hat{\mathbf{g}}_{q,j}^{(u)}\right]_0\\ \vdots&&&\vdots\\ \left[\hat{\mathbf{g}}_{q,j}^{(u)}\right]_{Q-2}&\left[\hat{\mathbf{g}}_{q,j}^{(u)}\right]_{Q-1}&\cdots&\\ \left[\hat{\mathbf{g}}_{q,j}^{(u)}\right]_{Q-1}&\left[\hat{\mathbf{g}}_{q,j}^{(u)}\right]_0&\cdots&\left[\hat{\mathbf{g}}_{q,j}^{(u)}\right]_{Q-2}\\ 0&\cdots&&0\\ \vdots&\cdots&&\vdots\\ 0&\cdots&&0\end{bmatrix},\tag{A.4}$$

and let $\mathbf{E}_{q,j}^{(u)}$ denote a $2Q\times Q$ matrix that is defined by

$$\begin{aligned}&\mathbf{E}_{q,j}^{(u)}\\ &=\begin{bmatrix}0&\cdots&0\\ \vdots&\cdots&\vdots\\ 0&\cdots&0\\ \left[\hat{\mathbf{g}}_{q,j}^{(u)}\right]_0\cdot e^{-j0\varphi^{(u)}}&\cdots&\left[\hat{\mathbf{g}}_{q,j}^{(u)}\right]_{Q-1}\cdot e^{-j(Q-1)\varphi^{(u)}}\\ \vdots&&0\\ \vdots&\iddots&\vdots\\ \left[\hat{\mathbf{g}}_{q,j}^{(u)}\right]_{Q-1}\cdot e^{-j(Q-1)\varphi^{(u)}}&0\quad\cdots&0\end{bmatrix}\\ &\cdot\boldsymbol{\Phi}_{L_U-L_G}^{(u)},\end{aligned}\tag{A.5}$$

Then, (A.2) can be expressed with the help of the matrices $\mathbf{C}_{q,j}^{(u)}$, $\mathbf{D}_{q,j}^{(u)}$, and $\mathbf{E}_{q,j}^{(u)}$ by

$$\begin{aligned}&\Big[\hat{\mathbf{g}}_{q,0}^{(u)\mathrm{H}}\cdot\boldsymbol{\mathcal{H}}^{(u)}+\hat{\mathbf{g}}_{q,1}^{(u)\mathrm{H}}\cdot\boldsymbol{\mathcal{H}}^{(u)}-\hat{\mathbf{g}}_{q,1}^{(u)\mathrm{H}}\cdot\boldsymbol{\Phi}_0^{(u)\mathrm{H}}\cdot\mathbf{H}_0^{(u)}\cdot\boldsymbol{\Phi}_0^{(u)},\\ &\hat{\mathbf{g}}_{q,1}^{(u)\mathrm{H}}\cdot\boldsymbol{\Phi}_0^{(u)\mathrm{H}}\cdot\mathbf{H}_0^{(u)}\cdot\boldsymbol{\Phi}_{L_U-L_G}^{(u)}+\hat{\mathbf{g}}_{q,2}^{(u)\mathrm{H}}\cdot\boldsymbol{\mathcal{H}}^{(u)}\Big]\\ &=\left[c_0^{(u)},\ldots,c_{Q-1}^{(u)},h_0^{(u)},\ldots,h_{Q-1}^{(u)}\right]^*\\ &\cdot\left[\mathbf{D}_{q,0}^{(u)}+\mathbf{D}_{q,1}^{(u)}-\mathbf{C}_{q,1}^{(u)},\ \mathbf{E}_{q,1}^{(u)}+\mathbf{D}_{q,2}^{(u)}\right].\end{aligned}\tag{A.6}$$

Thus, the $2Q \times 2Q$ matrices $\hat{\mathbf{g}}_q^{(u)}$, $q = 0, \ldots, Q-1$, are given by

$$\hat{\mathbf{g}}_q^{(u)} = \left[\mathbf{D}_{q,0}^{(u)} + \mathbf{D}_{q,1}^{(u)} - \mathbf{C}_{q,1}^{(u)},\ \mathbf{E}_{q,1}^{(u)} + \mathbf{D}_{q,2}^{(u)}\right]. \tag{A.7}$$

Acknowledgment

The authors would like to thank the anonymous reviewers for their helpful and supporting comments.

References

[1] ITU, "Requirements related to technical performance for IMT-Advanced radio interface(s)," Tech. Rep. ITU-R M.2134, International Telecommunication Union (ITU), Radiocommunication Sector, December 2008.

[2] R. van Nee and R. Prasad, *OFDM for Wireless Multimedia Communications*, Artech House, 1st edition, 2000.

[3] U. Sorger, I. De Broeck, and M. Schnell, "IFDMA—a new spread-spectrum multiple-access scheme," in *Proceedings of the of International Conference on Communications*, pp. 1013–1017, Atlanta, Ga, USA, June 1998.

[4] T. Frank, A. Klein, E. Costa, and E. Schulz, "IFDMA—a promising multiple access scheme for future mobile radio systems," in *Proceedings of the 16th IEEE International Symposium on Personal, Indoor and Mobile Radio Communications*, vol. 2, pp. 1214–1218, Berlin, Germany, September 2005.

[5] D. Galda, H. Rohling, E. Costa, H. Haas, and E. Schulz, "A low complexity transmitter structure for OFDM-FDMA uplink systems," in *Proceedings of the IEEE Vehicular Technology Conference*, vol. 4, pp. 1737–1741, Birmingham, UK, May 2002.

[6] WINNER, "Final report on identified RI key technologies, system concept, and their assessment," Tech. Rep. IST-2003-507581, D2.10 v1.0, December 2005, http://www.ist-winner.org/DeliverableDocuments/D2.10.pdf.

[7] T. Frank, A. Klein, and T. Haustein, "A survey on the envelope fluctuations of DFT precoded OFDMA signals," in *Proceedings of the IEEE International Conference on Communications (ICC '08)*, pp. 3495–3500, Beijing, China, May 2008.

[8] T. Frank, A. Klein, E. Costa, and A. Kuehne, "Low complexity and power efficient space-time-frequency coding for OFDMA," in *Proceedings of the IST Mobile and Wireless Communications Summit*, Mykonos, Greece, June 2006.

[9] A. Sohl, T. Frank, and A. Klein, "Channel estimation for DFT precoded OFDMA with blockwise and interleaved subcarrier allocation," in *Proceedings of the International OFDM Workshop*, Hamburg, Germany, 2006.

[10] A. Sohl and A. Klein, "Comparison of localized, interleaved and block-interleaved FDMA in terms of pilot multiplexing and channel estimation," in *Proceedings of the 15th European Signal Processing Conference*, Poznan, Poland, September 2007.

[11] L. Tong, G. Xu, and T. Kailath, "Blind identification and equalization based on second-order statistics: a time domain approach," *IEEE Transactions on Information Theory*, vol. 40, no. 2, pp. 340–349, 1994.

[12] M. K. Tsatsanis and G. B. Giannakis, "Transmitter induced cyclostationarity for blind channel equalization," *IEEE Transactions on Signal Processing*, vol. 45, no. 7, pp. 1785–1794, 1997.

[13] E. Moulines, P. Duhamel, J. F. Cardoso, and S. Mayrargue, "Subspace methods for the blind identification of multichannel FIR filters," *IEEE Transactions on Signal Processing*, vol. 43, no. 2, pp. 516–525, 1995.

[14] B. Muquet, M. de Courville, and P. Duhamel, "Subspace-based blind and semi-blind channel estimation for OFDM systems," *IEEE Transactions on Signal Processing*, vol. 50, no. 7, pp. 1699–1712, 2002.

[15] B. Muquet, M. de Courville, P. Duhamel, and V. Buzenac, "A subspace based blind and semi-blind channel identification method for OFDM systems," in *Proceedings of the 2nd IEEE Workshop on Signal Processing Advances in Wireless Communications*, pp. 170–173, Annapolis, Md, USA, May 1999.

[16] F. Gao and A. Nallanathan, "Blind channel estimation for OFDM systems via a generalized precoding," *IEEE Transactions on Vehicular Technology*, vol. 56, no. 3, pp. 1155–1164, 2007.

[17] A. Sohl and A. Klein, "Blind channel estimation based on second order statistics for IFDMA," in *Proceedings of the 19th International Symposium on Personal, Indoor and Mobile Radio Communications (PIMRC '08)*, Cannes, France, September 2008.

[18] A. Sohl and A. Klein, "Channel estimation for IFDMA—comparison of semiblind channel estimation approaches and estimation with interpolation filtering," in *Proceedings of the 20th IEEE Personal, Indoor and Mobile Radio Communications Symposium (PIMRC '09)*, Tokyo, Japan, September 2009.

[19] T. Svensson, T. Frank, D. Falconer, M. Sternad, E. Costa, and A. Klein, "B-IFDMA—a power efficient multiple access scheme for non-frequency-adaptive transmission," in *Proceedings of the 16th IST Mobile and Wireless Communications Summit*, pp. 1–5, Budapest, Hungary, July 2007.

[20] T. Svensson, T. Frank, T. Eriksson, D. Aronsson, M. Sternad, and A. Klein, "Block interleaved frequency division multiple access for power efficiency, robustness, flexibility and scalability," *EURASIP Journal on Wireless Communications and Networks*, vol. 2009, Article ID 720973, 18 pages, 2009.

[21] WINNERII, "The WINNER II air interface: refined multiple access concepts," Tech. Rep. IST-4-027756, D4.6.1 v1.0, November 2006, http://www.ist-winner.org/WINNER2-Deliverables/D4.6.1.pdf.

[22] K. Fazel and S. Kaiser, *Multi-Carrier and Spread Spectrum Systems*, John Wiley & Sons, New York, NY, USA, 1st edition, 2003.

[23] Z. Wang and G. B. Giannakis, "Wireless multicarrier communications: where Fourier meets Shannon," *IEEE Signal Processing Magazine*, vol. 17, no. 3, pp. 29–48, 2000.

[24] T. Frank, A. Klein, E. Costa, and E. Schulz, "Low complexity equalization with and without decision feedback and its application to IFDMA," in *Proceedings of the 16th IEEE International Symposium on Personal, Indoor and Mobile Radio Communications*, vol. 2, pp. 1219–1223, Berlin, Germany, September 2005.

[25] M. Schnell and I. De Broeck, "Application of IFDMA to mobile radio transmission," in *Proceedings of the IEEE International Conference on Universal Personal Communications*, vol. 2, pp. 1267–1272, Florence, Italy, October 1998.

[26] G. H. Golub and C. F. van Loan, *Matrix Computations*, The John Hopkins Universtiy Press, 3rd edition, 1996.

[27] W. Li, O. Takyu, K. Adachi, and M. Nakagawa, "Performance evaluation of decision directed channel estimation for single user IFDMA," in *Proceedings of the IEEE Radio and Wireless Symposium (RWS '08)*, pp. 659–662, Orlando, Fla, USA, January 2008.

[28] A. Guha and K. Giridhar, "Enhanced channel estimation and tracking for single carrier uplink transmission scheme," in *Proceedings of the National Conference on Communications*, Mumbai, India, 2008.

[29] C. T. Lam, D. D. Falconer, and F. Danilo-Lemoine, "A low complexity frequency domain iterative decision-directed channel estimation technique for single-carrier systems," in *Proceedings of the 65th IEEE Vehicular Technology Conference (VTC '07)*, pp. 1966–1970, Dublin, Ireland, April 2007.

[30] M. H. Hayes, *Statistical Digital Signal Processing and Modeling*, John Wiley & Sons, New York, NY, USA, 1st edition, 1996.

[31] M. Paetzold, *Mobile Fading Channels*, John Wiley & Sons, New York, NY, USA, 1st edition, 2002.

[32] W. Koch and A. Baier, "Optimum and sub-optimum detection of coded data disturbed by time-varying intersymbol interference [applicable to digital mobile radio receivers]," in *Proceedings of the IEEE Global Telecommunications Conference*, vol. 3, pp. 1679–1684, December 1990.

[33] P. Robertson, E. Villebrun, and P. Hoeher, "A Ccomparison of optimal and sub-optimal MAP decoding algorithms operating in the log domain," in *Proceedings of the IEEE International Conference on Communications*, vol. 2, pp. 1009–1013, Seattle, Wash, USA, June 1995.

[34] H. Sari, G. Karam, and I. Jeanclaud, "Frequency-domain equalization of mobile radio and terrestrial broadcast channels," in *Proceedings of the IEEE Global Telecommunications Conference*, vol. 1, pp. 1–5, San Francisco, Calif, USA, November-December 1994.

[35] WINNERII, "WINNER II Channel Models, Part I Channel Models," Tech. Rep. IST-4-027756, D1.1.2, v1.1, February 2008, http://www.ist-winner.org/WINNER2-Deliverables/D1.1.2v1.1.pdf.

[36] K. D. Kammeyer and K. Kroschel, *Digitale Signalverarbeitung: Filterung und Spektralanalyse*, B.G. Teubner, Stuttgart, Germany, 4th edition, 1998.

Preliminary call for papers

The 2011 European Signal Processing Conference (EUSIPCO-2011) is the nineteenth in a series of conferences promoted by the European Association for Signal Processing (EURASIP, www.eurasip.org). This year edition will take place in Barcelona, capital city of Catalonia (Spain), and will be jointly organized by the Centre Tecnològic de Telecomunicacions de Catalunya (CTTC) and the Universitat Politècnica de Catalunya (UPC).

EUSIPCO-2011 will focus on key aspects of signal processing theory and applications as listed below. Acceptance of submissions will be based on quality, relevance and originality. Accepted papers will be published in the EUSIPCO proceedings and presented during the conference. Paper submissions, proposals for tutorials and proposals for special sessions are invited in, but not limited to, the following areas of interest.

Areas of Interest

- Audio and electro-acoustics.
- Design, implementation, and applications of signal processing systems.
- Multimedia signal processing and coding.
- Image and multidimensional signal processing.
- Signal detection and estimation.
- Sensor array and multi-channel signal processing.
- Sensor fusion in networked systems.
- Signal processing for communications.
- Medical imaging and image analysis.
- Non-stationary, non-linear and non-Gaussian signal processing.

Submissions

Procedures to submit a paper and proposals for special sessions and tutorials will be detailed at www.eusipco2011.org. Submitted papers must be camera-ready, no more than 5 pages long, and conforming to the standard specified on the EUSIPCO 2011 web site. First authors who are registered students can participate in the best student paper competition.

Important Deadlines:

Proposals for special sessions	15 Dec 2010
Proposals for tutorials	18 Feb 2011
Electronic submission of full papers	**21 Feb 2011**
Notification of acceptance	23 May 2011
Submission of camera-ready papers	6 Jun 2011

Webpage: www.eusipco2011.org

Organizing Committee

Honorary Chair
Miguel A. Lagunas (CTTC)

General Chair
Ana I. Pérez-Neira (UPC)

General Vice-Chair
Carles Antón-Haro (CTTC)

Technical Program Chair
Xavier Mestre (CTTC)

Technical Program Co-Chairs
Javier Hernando (UPC)
Montserrat Pardàs (UPC)

Plenary Talks
Ferran Marqués (UPC)
Yonina Eldar (Technion)

Special Sessions
Ignacio Santamaría (Unversidad de Cantabria)
Mats Bengtsson (KTH)

Finances
Montserrat Nájar (UPC)

Tutorials
Daniel P. Palomar (Hong Kong UST)
Beatrice Pesquet-Popescu (ENST)

Publicity
Stephan Pfletschinger (CTTC)
Mònica Navarro (CTTC)

Publications
Antonio Pascual (UPC)
Carles Fernández (CTTC)

Industrial Liaison & Exhibits
Angeliki Alexiou (University of Piraeus)
Albert Sitjà (CTTC)

International Liaison
Ju Liu (Shandong University-China)
Jinhong Yuan (UNSW-Australia)
Tamas Sziranyi (SZTAKI -Hungary)
Rich Stern (CMU-USA)
Ricardo L. de Queiroz (UNB-Brazil)